Technological University Dublin
ARROW@TU Dublin

Articles | Centre for Industrial and Engineering Optics

2015

Photonic Hydrogel Sensors

Ali K. Yetisen
Harvard Medical School, Wellman Center for Photomedicine, Massachusetts General Hospital, USA

Haider Butt
School of Mechanical Engineering, University of Birmingham, Birmingham, United Kingdom

Lisa R Volpatti
Department of Chemical Engineering, Massachusetts Institute of Technology, Cambridge, USA

See next page for additional authors

Follow this and additional works at: https://arrow.tudublin.ie/cieoart

 Part of the Medicine and Health Sciences Commons

Recommended Citation

Yetisen, A.K., Butt, H. & Volpatt, L.R. (2016). Photonic hydrogel sensors. *Biotechnology Advances*, vol. 34, no. pg. 250-271. doi:10.1016/j.biotechadv.2015.10.005

This Article is brought to you for free and open access by the Centre for Industrial and Engineering Optics at ARROW@TU Dublin. It has been accepted for inclusion in Articles by an authorized administrator of ARROW@TU Dublin. For more information, please contact arrow.admin@tudublin.ie, aisling.coyne@tudublin.ie, gerard.connolly@tudublin.ie.

This work is licensed under a Creative Commons Attribution-Noncommercial-Share Alike 4.0 License

Authors

Ali K. Yetisen, Haider Butt, Lisa R Volpatti, Ida Pavlichenko, Matjaž Humar, Sheldon J.J.Kwok Sheldon J.J.Kwok, Heebeom Koo, Ki Su Kim, Izabela Naydenova, Ali Khademhosseini, Sei Kwang Hahnk, and Seok Hyun Yunaf

This article is available at ARROW@TU Dublin: https://arrow.tudublin.ie/cieoart/85

ResearchGate

See discussions, stats, and author profiles for this publication at: https://www.researchgate.net/publication/283048726

Photonic hydrogel sensors

Article *in* Biotechnology advances · October 2015

DOI: 10.1016/j.biotechadv.2015.10.005

CITATIONS
61

READS
1,716

12 authors, including:

Haider Butt
Khalifa University
173 PUBLICATIONS **2,170** CITATIONS
SEE PROFILE

Matjaž Humar
Jožef Stefan Institute
43 PUBLICATIONS **1,215** CITATIONS
SEE PROFILE

Ki Su Kim
Pusan National University
52 PUBLICATIONS **2,218** CITATIONS
SEE PROFILE

Izabela Naydenova
Technological University Dublin - City Campus
160 PUBLICATIONS **2,020** CITATIONS
SEE PROFILE

Some of the authors of this publication are also working on these related projects:

Project Development of holographic sensors for monitoring relative humidity and temperature View project

Project FOCAS Research Institute View project

All content following this page was uploaded by Haider Butt on 29 November 2015.

The user has requested enhancement of the downloaded file.

Biotechnology Advances Special Issue: Trends in IVD and Mobile Healthcare

Photonic Hydrogel Sensors

Ali K. Yetisen[1,*], *Haider Butt*,[2] *Lisa R. Volpatti*,[3] *Ida Pavlichenko*,[4] *Matjaž Humar*,[1,5] *Sheldon J. J. Kwok*[1,6], *Heebeom Koo*,[1] *Ki Su Kim*,[1] *Izabela Naydenova*,[7] *Ali Khademhosseini*,[6,8] *Sei Kwang Hahn*,[9] and *Seok Hyun Yun*[1,6,*]

[1] Harvard Medical School and Wellman Center for Photomedicine, Massachusetts General Hospital, 65 Landsdowne Street, Cambridge, Massachusetts 02139, USA

[2] School of Mechanical Engineering, University of Birmingham, Edgbaston, Birmingham B15 2TT, United Kingdom

[3] Department of Chemical Engineering, Massachusetts Institute of Technology, 77 Massachusetts Avenue, Cambridge, Massachusetts 02139, USA

[4] School of Engineering and Applied Sciences, Harvard University, 9 Oxford Street, Cambridge, MA 02139, USA

[5] Condensed Matter Department, J. Stefan Institute, Jamova 39, SI-1000 Ljubljana, Slovenia

[6] Harvard-MIT Division of Health Sciences and Technology, Massachusetts Institute of Technology, Cambridge, Massachusetts 02139, USA

[7] Centre for Industrial and Engineering Optics, School of Physics, College of Sciences and Health, Dublin Institute of Technology, Dublin 8, Ireland

[8] Biomaterials Innovation Research Center, Division of Biomedical Engineering, Brigham and Women's Hospital, Harvard Medical School, Cambridge, Massachusetts, 02139, USA; Wyss Institute for Biologically Inspired Engineering, Harvard University, Boston, Massachusetts 02115, USA; Department of Physics, King Abdulaziz University, Jeddah, Saudi Arabia

[9] Department of Materials Science & Engineering, Pohang University of Science and Technology (POSTECH), 77 Cheongam-ro, Nam-gu, Pohang, Kyungbuk 790-784, Korea

* corresponding authors (ayetisen@mgh.harvard.edu, syun@mgh.harvard.edu)

Abstract

Analyte-sensitive hydrogels that incorporate optical structures have emerged as sensing platforms for point-of-care diagnostics. The optical properties of the hydrogel sensors can be rationally designed and fabricated through self-assembly, microfabrication or laser writing. The advantages of photonic hydrogel sensors over conventional assay formats include label-free, quantitative, reusable, and continuous measurement capability that can be integrated with equipment-free text or image display. This review explains the operation principles of photonic hydrogel sensors, presents syntheses of stimuli-responsive polymers, and provides an overview of qualitative and quantitative readout technologies. Applications in clinical samples are discussed, and potential future directions are identified.

Keywords: hydrogels; in vitro diagnostics; photonic crystals; inverse opals; holography; Bragg stacks; crystalline colloidal arrays; block copolymers; layer-by-layer deposition; plasmonics

Contents

1. Introduction

1.1 The Need for Photonic Sensors

The *in vitro* diagnostics (IVD) market was valued at $53.3 B in 2013 and projected to reach $69.1 B by 2017 (Markets&Markets, 2013, Shields and Sale, 2014). While the global IVD market is expected to grow at a compound annual growth rate (CAGR) of 5.4% until 2020, the emerging markets (Brazil, China, and India) are projected to experience 10-15% growth (GrandViewResearch, 2014, Park, 2014, Rosen, 2014). This growth is mainly driven by (i) the shift to personalized medicine, (ii) the need for minimally invasive rapid diagnostics, (iii) aging populations in the developed world, and (iv) geographical market expansion and the increase in the demand from emerging economies due to infectious and chronic diseases (Akram et al. , 2015, Yetisen et al. , 2015b). Although the market is restrained by stringent regulations (Mansfield et al. , 2005), there is a growing number of commercial products such as diagnostic tests for HIV, hepatitis, HPV, diabetes, blood coagulation, fertility, immunoassays, hematology, urinalysis, molecular diagnostics, and blood gas analyses (Roche, 2014, Siemens, 2014).

The fastest growing segments of the IVD market are molecular diagnostics and point-of-care (POC) testing, which attracted $650 million in investments over the past five years (KaloramaInformation, 2014, Parmar, 2013, St John and Price, 2014). The expansion of POC diagnostics may be attributed to the government policies to reduce high-cost healthcare provisions by decreasing the number of patients in secondary and tertiary hospitals (Price and Kricka, 2007). POC diagnostics consist of small benchtop or handheld devices that provide qualitative and semi-quantitative information of target analytes in the field or at home (Chin et al. , 2012). Benchtop products include critical care analyzers, as well as hematology and immunology assays. Handheld devices consist of blood glucose tests, dipsticks for urinalysis and lateral-flow tests (Yetisen et al. , 2013). These handheld devices are simple, rapid, robust in storage and usage, and low cost. Thus, they are universally applicable for disposable and sensitive point-of-care diagnostics. The sensing mechanisms of handheld point-of-care diagnostics are based on molecular probes, enzymes, antibody-antigen interactions, and

electrochemistry. Dipstick tests such as urine test strips utilize molecular dyes and enzymatic reactions. Such assays are multiplexed and allow the analyses of up to 12 biomarkers. Recently, new capabilities have been proposed for these formats to execute multistep processes (Cate et al. , 2015). A significant limitation of assays based on molecular dyes is that they have different absorption peaks in the visible spectrum (Martinez et al. , 2008). The interpretation of such assays may be erroneous due to the subjective readouts of calibration charts and uneven development of colors throughout the assay. Their semi-quantitative readouts require handheld analyzers. Additionally, the number of analytes and molecular reactions that can be combined with chromogens is limited. Hence, standardization of color shift in the visible spectrum and expansion to a broad range of analytes are significant challenges in molecular dye based assays (Yetisen, 2015f). Furthermore, while the colorimetric information is universal, some applications require written readouts for reporting the concentration of a target analyte. The lateral-flow format is typically based on immunochromatography involving immobilized antibodies and functionalized gold nanoparticles, which were originally designed for qualitative readouts. Recently, newer capabilities were introduced to this platform to obtain semi-quantitative readouts. For example, ClearblueDigital Pregnancy Test (Swiss Precision Diagnostics) offers on-chip quantification of chorionic gonadotropin (hCG) to estimate the conception date (Pike et al. , 2013). Among the over the counter products, blood glucose monitoring is the largest market segment due the prevalence of 382 million diagnosed diabetics worldwide (Danaei et al. , 2011, DiabetesAtlas, 2013). Glucose assays are based on enzymes such as glucose oxidase (GOx), glucose dehydrogenase (GDH) or hexokinase, which are read out by handheld devices. However, such electrochemical and enzymatic assays are prone to error due to interference from high partial pressure of oxygen, maltose, and hematocrit (Tonyushkina and Nichols, 2009). Additionally, these assays do not allow real-time or on-demand reusable measurements due to the irreversibility of reactions and assay configurations. The development of all-in-one platforms that can report on the concentrations of target analytes by either utilizing the entire visible spectrum, or producing written information or display images without electrical components are needed to create low-cost, robust and quantitative point-of-care diagnostics.

The limitations of the existing sensors have motivated the investigation of label-free structural color platforms that quantitatively report on the concentration of target analytes (Zhao et al. , 2010a). Structural coloration was first observed by Robert Hooke and Isaac Newton in peacock feathers and mother of pearl (nacre) (Hooke, 1665, Newton, 1704). To understand structural coloration, Thomas Young demonstrated that light could behave like a wave, producing diffraction from sharp edges or slits (Young, 1804). A wide array of mechanisms has evolved to create diverse optical structures, including multilayer reflectors, photonic crystals, and light scattering structures (Fudouzi, 2011, Zhao et al. , 2012). These structural colors also coincidentally form in composite and fibrous structures (Martinez-Hurtado et al. , 2013, Vignolini et al. , 2012, Vukusic and Sambles, 2003). Structural coloration in nature occurs mainly through diffraction, but also refraction, plasmonics, or a combination of both, sometimes complementing pigments. The fundamentals of dynamic coloration in photonic structures in nature represent a potential for constructing transducers that can be modulated by physical changes.

Structural color-based transducers have advantages over traditional signal processing approaches in terms of response-range tuning and label-free reporting. Advances in photography, polymer chemistry, laser physics, and organic synthesis have enabled bottom-up and top-down fabrication of photonic structural colors. Hence, the developments in photonic structures have set

the stage for the incorporation of structural colors in analyte-sensitive hydrophilic polymers (hydrogels) for sensing applications. In contrast to the absorption of light by chromophores and electrochemistry, photonic hydrogel sensors incorporate nanostructures that modulate the optical properties of incident light. Such photonic structures can be created in/on hydrogels through self-assembly or laser writing techniques. Upon interacting with a target analyte, hydrogels undergo volumetric changes, which affect the physical and/or optical properties of the photonic structures. These photonic structures serve as transducers to quantify the concentration of analytes through changes in spatial periodicity in their dielectric constants, plasmonic resonance shifts, or effective refractive index. They typically modulate the optical characteristics of electromagnetic waves by filtering out certain regions of wavelengths, a phenomenon called the photonic band gap (PBG), which typically occurs in 1D Bragg gratings as well as 2D and 3D colloidal photonic crystals (Joannopoulos et al. , 2011). However, the filtering mechanism of these sensors may include Fabry-Pérot interferometer (etalon), or thin film effects.

This Review presents the operation principles of photonic hydrogel sensors. It describes the syntheses of analyte-sensitive hydrogel matrixes and explains bottom-up and top-down nano/microfabrication methods to incorporate structures within hydrogels that act as optical transducers. The technical challenges in sensor fabrication are identified, and pre-clinical and clinical performance evaluations are presented. This Review also discusses how photonic hydrogel sensors can address IVD market needs. The perceived limitations of photonic hydrogel sensors in building commercial products are identified, and potential future directions are described.

1.2 Historical Development of Diffraction Gratings in Hydrogels

Experimentation with gels in optics began in the 19th century. Frederick Archer invented the collodion process, which utilized albumen (egg white) photographic prints (Archer, 1851, Blanquart-Evrard, 1847). To improve the collodion process, Richard Maddox reported a method to create photographic images in gelatin (Maddox, 1871). Two decades later, Gabriel Lippmann introduced a technique to create color photographs based on interference of light (Lippmann, 1894). Lippmann projected an image onto a silver bromide containing photographic emulsion, which was backed by a mirror of liquid mercury. The light reflected back by the mirror created standing waves in the emulsion. This latent image was later photographically developed to produce periodic silver planes. When illuminated with a broadband light source, the Lippmann plate replayed a colored image via diffraction. After the development of the principle of holography in the 1940s (Gabor, 1948, Gabor, 1949) and invention of laser in the 1950s (Maiman, 1960), Yuri Denisyuk of the former Soviet Union, and Emmett Leith and Juris Upatnieks in the United States created 3D holographic gratings in gelatin in the 1960s (Denisyuk, 1962, Leith and Upatnieks, 1962). In parallel to the developments in holography, hydrogel chemistry also made significant advances (Loh and Scherman, 2012). Poly(*N*-isopropylacrylamide) polyacrylamide were first synthesized in Rohm & Haas Company (Philadelphia, PA) (Specht et al. , 1956); however, its thermal expansion properties in aqueous solutions was realized after a decade (Heskins and Guillet, 1968). In the former Czechoslovakia, Otto Wichterle and Drahoslav Lím developed poly(2-hydroxyethyl methacrylate) (pHEMA) for application in soft contact lenses (Wichterle and Lim, 1960).

The advantages of incorporating diffraction gratings in polymers matrixes have been realized by Thomson-CSF (France) (Loiseaux et al. , 1984). This approach involved forming a medium consisting of suspended dielectric nanoparticles (~20 nm) in a monomer solution. Standing

waves consisting of high (antinodes) and low (nodes, no disturbance) energy induced by holographic optical forces moved the nanoparticles into periodic regions. Subsequently, nanoparticles were fixed to their positions by polymerizing the monomer solution. It was not until 1990s that the use of holographic gratings in biosensing applications was proposed by Christopher R. Lowe at the University of Cambridge (Lowe et al. , 1995). Holograms were used as recording media to create diffraction gratings in functionalized hydrogel matrixes and the principle of operation of hydrogel-based optical sensors was demonstrated. Independently Sanford Asher at the University of Pittsburgh have developed crystalline colloidal arrays (CCAs) for narrow-band filtering devices in the visible spectrum and UV (Asher, 1986). In their earlier work, the liquid dispersion was contained in a thin planar cell within walls of transparent plastics or glass. However, a significant challenge with the utilization of the CCAs was their fragility, and the arrays were affected from vibration, temperature changes, and ionic influences. Hence, in the 1990s, CCAs have been incorporated in hydrogel films (Haacke et al. , 1993). Based on this platform, Asher and co-workers developed hydrogel sensors based on CCAs (Asher and Holtz, 1998). Hence, along with the advances in recognition agents, photonic hydrogel sensors opened up opportunities for *in vitro* diagnostics.

1.3 The Prospects for Photonic Hydrogel Sensors

Photonic structures embedded in hydrogels that change their water content and volume upon interacting with a specific analyte represent a new platform to construct IVD devices. Hydrogels are 3D polymer networks capable of undergoing reversible volume changes as their Donnan osmotic pressure changes (Imran et al. , 2010, Miyata, 2010). Hydrogels can be synthesized to be sensitive to a range of clinically relevant analytes (Banwell et al. , 2009, Cai et al. , 2015, Ehrbar et al. , 2008, Ehrick et al. , 2005, Kloxin et al. , 2009, Lendlein et al. , 2005, Stuart et al. , 2010, Um et al. , 2006). These hydrogels consist of bioactive recognition molecules that selectively respond to external stimuli via producing physical or chemical changes in the hydrogel matrix (Buenger et al. , 2012, Loh and Scherman, 2012). Functionalized hydrogels can be used as a medium to incorporate photonic structures for optical signal transduction and reporting within one device. Numerous bottom-up or top-down nano/microfabrication methods have been developed to create photonic structures in miniaturized and multiplexed formats (Zhao, Zhao, 2010a). Upon interacting with a target analyte, the volumetric change in the hydrogel is reported through modulations of reflection, diffraction, refraction, surface plasmon resonance, or emission (Gerlach and Arndt, 2009). These optical changes act as a transducer, allowing various light properties to be analyzed spectroscopically and correlated with the concentration of the analyte. Additionally, photonic hydrogel sensors can be tuned to report visually-distinguishable color changes that can be semi-quantitatively determined without equipment. The most important advantage of photonic hydrogel sensors over established assay formats is that they do not rely on labels or electrochemistry to report on the concentration of a target analyte; hence, they are immune to marker bleaching, signal drifts, and electromagnetic interference. Photonic hydrogel sensors (i) incorporate functionalized polymers to respond to a target analyte, (ii) offer reversible real-time measurement of analytes, (iii) can be tuned to report the concentration of analytes colorimetrically from ultraviolet to near-infrared, and (iv) are compatible with readout devices for quantitative measurements. These photonic hydrogels may also have optically active elements with capabilities in displaying three-dimensional (3D) images or writing (Naydenova et al. , 2008). Hence, the development of photonic hydrogel sensors has immense potential for both

equipment-free semi-quantitative diagnostics and quantitative analyzers that are compatible with mobile spectrophotometers and smartphone readers (Burgess et al. , 2013, Yetisen, 2015e).

The potential applications of photonic hydrogel sensors are not limited to medical diagnostics, but also include veterinary testing, pharmaceutical bioassays, and biohazard and environmental monitoring. However, the main focus area of hydrogel sensors has been in the detection and/or quantification of chemicals and cells in medical diagnostics. For example, their potential applications in biochemistry and biology are monitoring enzyme activity and metabolites (Tian et al. , 2014), and serum albumin ligand binding (Cai et al. , 2014). Another potential area of application of photonic hydrogel sensors includes the detection of biocontaminants, heavy metals, and nanoparticles in water or air. The development of environmental sensors is aligned with the strict regulations imposed by the European Union, the United States, and other countries as well as companies operating in the developing world. Reusable hydrogel-based sensing of environmental contaminants is an emerging area that can significantly reduce the costs and turnaround time at resource-limited settings.

2. Photonic Band-Gap Hydrogels

Bragg diffraction of light from nanoscale periodic structures can be designed to be dependent on the presence of analytes in a controlled way and therefore can be employed to create sensors reporting from ultraviolet to near-infrared (Ge and Yin, 2011). Periodic structures within hydrogel matrixes can be formed using nanostructures, or can consist of different block copolymers or layers of polyelectrolytes. The specificity of such sensors is achieved by functionalizing the hydrogel matrix with chelating agents or ligands pre- or post-polymerization (Zhao, Zhao, 2010a). Bottom-up and top-down fabrication techniques include laser-directed writing of gratings (Yetisen et al. , 2014f), colloidal self-assembly (Cai, Smith, 2015), pore etching (DeLouise et al. , 2005), spincoating (von Freymann et al. , 2013), block-co-polymerization (Kim et al. , 2010), and layer-by-layer deposition (Kotov, 1999).

2.1. Holographic Sensors

Holograms can be used as analytical devices to quantify the humidity content and biomolecule concentration (Blyth et al. , 1996, Lowe, Millington, 1995, Millington et al. , 1996, Spooncer et al. , 1992). Holographic sensors incorporate multilayer Bragg diffraction gratings in functionalized hydrogel matrixes. Altering the lattice spacing, the effective refractive index, and/or the refractive index modulation of the Bragg grating changes the characteristics of the diffracted or transmitted light (Yetisen, 2015a). For example, in reflection holograms, swelling or shrinking of the polymer matrix shifts the Bragg peak to longer or shorter wavelengths, and the change in the position of the Bragg peak is correlated with the concentration of the analyte that is being measured (Figure 1a). The diffraction grating in the hologram acts as a reporter allowing changes in the color to be monitored semi-quantitatively by eye, or quantitatively using a spectrophotometer or a smartphone camera. The advantage of holographic sensors over other photonic hydrogel sensors is the ability to accurately fabricate the structure via tuning the optical properties of the Bragg grating using laser light.

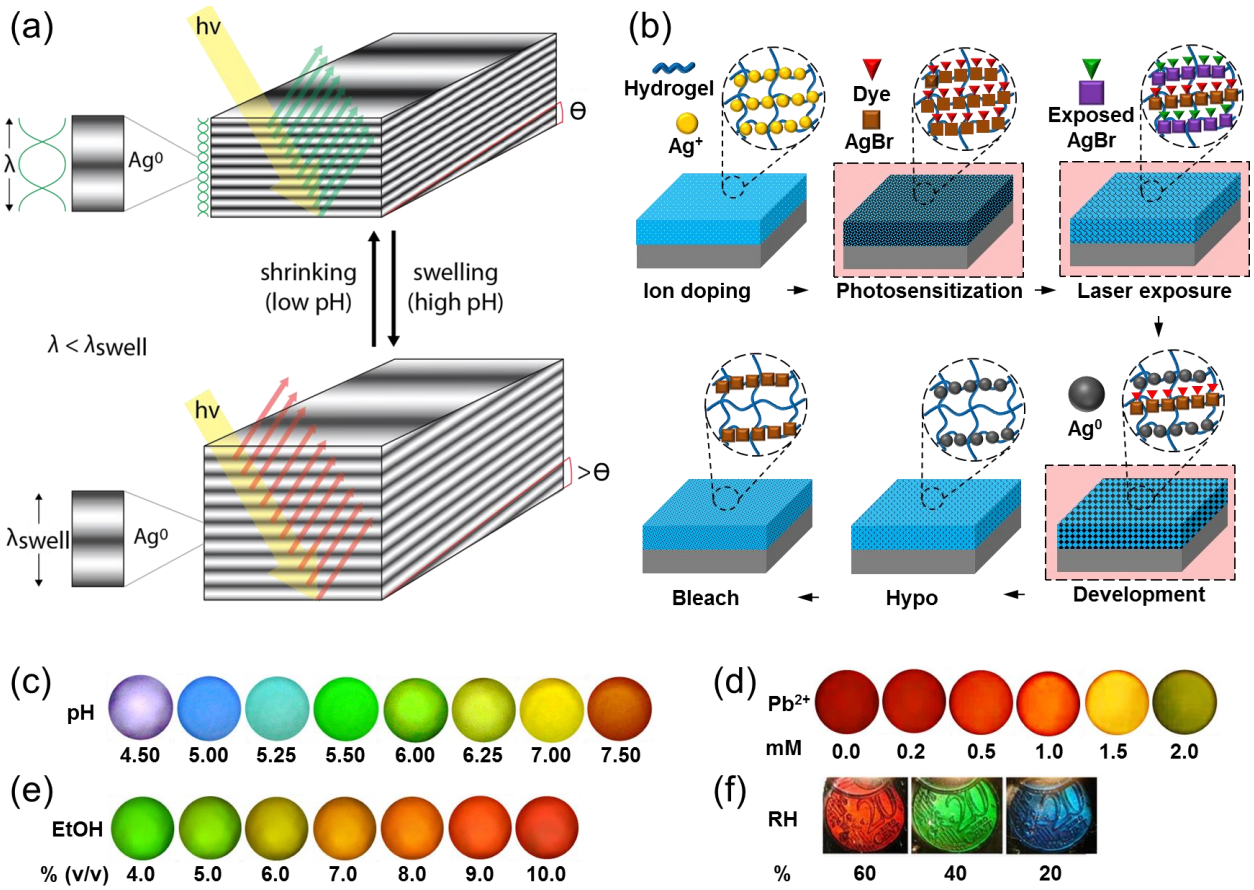

Figure 1. Holographic sensors. (a) The modulation of Bragg diffraction gratings in reflection holographic sensors as a function of pH. An increase in pH swells the hydrogel matrix and expands the lattice spacing of the grating, shifting the diffracted light to longer wavelengths. (b) Fabrication of holographic sensors by silver halide chemistry and laser writing. (c) Colorimetric response of holographic carboxylated pHEMA pH sensor. Reprinted with permission from (Yetisen et al. , 2014a). Copyright, Wiley-VCH Verlag GmbH&Co. KGaA, Weinheim. (d) 8-hydroxyquinoline-functionalized Pb^{2+} ions. Reprinted with permission from (Yetisen et al. , 2015a). Copyright, American Chemical Society. (e) pHEMA ethanol sensor. Reprinted with permission from (Yetisen et al. , 2014g), Copyright, The Royal Society of Chemistry. (f) Poly(acrylamide-*co*-vinylalcohol) humidity sensor with image displaying capabilities. Reprinted with permission from (Naydenova, Jallapuram, 2008) Copyright, American Institute of Physics.

The design of a holographic sensor involves determining (i) monomers to construct a hydrogel matrix, (ii) a bioactive recognition group, and (iii) an image recording technique (Yetisen, 2015d). Commonly used monomers include 2-hydroxyethyl methacrylate (HEMA), acrylamide (AAM), vinyl alcohol (VA), and siloxane. These monomers can be polymerized over a silanized glass or an O_2 plasma-treated plastic substrate in the presence of crosslinkers using photo or thermal initiators such as 2,2-dimethoxy-2-phenylacetophenone (DMPA) and *N*,*N*,*N*′,*N*′-tetramethylethylenediamine (TEMED) (Tsangarides et al. , 2014). A range of functional groups can be added to the monomer mixture to create specificity for target analytes. Potential functional groups include carboxylic acid, crown ethers, 8-hydroxyquinoline, porphyrin and phenyl boronic acid derivatives (Kabilan et al. , 2004, Marshall et al. , 2003, Mayes et al. , 2002, Yetisen, Qasim, 2014g). Functional groups can also be introduced after polymerization

through a DCC-initiated condensation reaction by forming amide linkages (Yetisen, Montelongo, 2015a). Alternatively, sensitivity to analytes can also be achieved by introducing nanoparticles (zeolites) to the monomer mixture (Leite et al. , 2010a, Leite et al. , 2010b, Zaarour et al. , 2014).

The fabrication of holographic sensors involves forming diffraction gratings in the hydrogel matrix. Depending on the hydrophilicity of the polymer matrix, silver halide chemistry, high-energy laser patterning, or photopolymerization can be used to record the photonic structure. The early holographic sensors were recorded by silver halide chemistry (Millington, Mayes, 1996). In gelatin emulsions, silver halides are prepared when the gelatin is molten in aqueous conditions, and coated over a substrate as thin film. However, this strategy is not universally applicable due to the immiscibility of some monomer species with water. Hence, a diffusion method was developed for doping the hydrogel matrixes with Ag^{+} ions (Blyth et al. , 1999). Typically, under safelighting, Ag^{+} ions are converted to AgBr nanocrystals using aqueous LiBr in the presence of photosensitizers (Marshall, Blyth, 2003). Subsequently, the recording medium is exposed to laser light to produce a latent image, which can be later converted to Ag^{0} nanoparticles using a photographic developer (Figure 1b).

Holographic sensors can also be recorded by using intense pulses of laser light (Yetisen et al. , 2014e). For example, high-energy frequency doubled Nd:YAG (Nd-Yttrium-Aluminum-Garnet) ns pulsed lasers or other high-energy lasers can be used to create reflection holograms (Martinez-Hurtado et al. , 2010). The typical laser energy output of such lasers is 300 mJ with a pulsed laser operating at 532 nm. However, low-cost Q-switched lasers for tattoo removal can also be used. In contrast to silver halide holography, high-energy patterning does not require formation of silver halide nanocrystals. This fabrication method consists of the impregnation of the hydrogel matrix with a light-absorbing material and laser exposure of the recording media to form diffraction gratings, allowing the use of any light-absorbing material in the hydrogel matrix. For example, Ag^{+} ions can be perfused into the hydrogel matrix, and reduced *in situ* using a photographic developer to Ag^{0} nanoparticles (Ø=50-100 nm). Nanoparticles of this size absorb in a wavelength range overlapping with the laser emission wavelength at 532 nm. Similarly, other metal nanoparticles (*i.e.* gold or iron), pigments, dyes, and carbon nanotubes can be used to produce the gratings (Vasconcellos et al. , 2014, Zhao et al. , 2015a). The interaction of laser light with nanoparticles might result in reduction in particle size, oxidation, modification in the crystal structure or morphology, further crosslinking, or diffusion in the antinode or node regions, which may contribute to reorganizing the nanoparticles in the hydrogel matrix (Yetisen, Butt, 2014a).

Holographic sensors can also be constructed using photopolymers (Mikulchyk et al. , 2014). A significant advantage of photopolymers over silver halide chemistry and high-energy patterning is the ability to achieve high diffraction efficiency. Photopolymer-based holographic sensors are typically constructed from acrylamide and vinyl alcohol (Mikulchyk et al. , 2013, Naydenova, Jallapuram, 2008, Naydenova et al. , 2009). To fabricate the hologram, a mixture of monomers, crosslinker, photoinitiator and sensitizers are coated over a substrate. The resulting hydrogel matrix is exposed to an interference pattern to create a multilayer photonic structure. When the light is absorbed at the antinode regions of the standing wave, the monomers undergo free radical chain polymerization. Hence, this process locally changes the refractive index and the polarization of the molecules. The spatial variation in the intensity of the interference pattern is recorded as a variation of refractive index.

Holographic sensors have been utilized to sense ions, metabolites, enzymes, drugs, microorganisms, and other clinically relevant stimuli (Yetisen, Naydenova, 2014f) (Table 1).

Earlier research in holographic sensors focused on the development of pH sensors (Marshall, Blyth, 2003). Functionalization with acidic or basic groups allowed the hydrogel matrix to swell and shrink due to the change in Donnan osmotic pressure as the pH of the system was varied (Figure 1c). The monomers that can be incorporated in holographic pH sensors include methacrylic acid (MAA), trifluoromethyl propenoic acid (TFMPA), dimethylaminoethyl methacrylate (DMAEM), and vinyl imidazole to detect the pH from 2.0 to 9.0 to achieve 0.01 pH unit sensitivity. A limitation of these hydrogel-based pH sensors is that they are affected by changes in ionic strength. Holographic sensors can also be utilized in the quantification of mono/divalent metal ions for the detection of electrolytes in clinical chemistry.

Holographic sensors were functionalized with methacrylated crown ethers to sense K^+ ions (Mayes, Blyth, 2002). A holographic sensor containing 18-crown-6 (50 mol%) allowed sensing K^+ ions (≤30 mM) within 30 s. Recently, newer receptors such as porphyrin derivatives were incorporated into holographic sensors for the detection of divalent metal ions (Yetisen, Qasim, 2014g). Holographic sensors consisting of porphyrin derivatives as chelating agents responded to Cu^{2+} and Fe^{2+} ions within the concentration range of 0.05-1.00 mM in 30 s. However, these sensors were insensitive to divalent metal ions below 10 mM (Yetisen, 2015c). The same sensors were also used to sense alcohols as the concentration of ethanol was varied from 4 to 10 % (v/v) (Figure 1d). Another recent holographic sensor featuring 8-hydroxyquinoline (8HQ) as a chelating agent for Pb^{2+} ions was shown to have a dynamic range of 0.1-10.0 mM with a limit of detection of 11.4 μM (Figure 1e) (Yetisen, Montelongo, 2015a). Holographic sensors incorporating boronic acid derivatives were shown to be sensitive to glucose. 3-(acrylamido)phenylboronic acid (3-APB) (pK_a = ~8.8) binds to carbohydrates by forming reversible covalent bonds through its *cis*-diol units (Kabilan, Blyth, 2004, Kabilan et al. , 2005). The principle of operation was based on the change in Donnan osmotic pressure, which shifts the Bragg peak to longer wavelengths in the presence of carbohydrates (Yetisen, 2015b).

Holographic sensors also have the capability to incorporate images (Naydenova, Jallapuram, 2008). Holographic humidity sensors were fabricated in acrylamide photopolymer in Denisyuk reflection mode (Figure 1f). After breathing over the holographic sensor, the change in the diffracted light provided a qualitative and quantitative readout of the relative humidity (RH) in the environment. The color change was observed within seconds after changing the RH, and this process was reversible. Images can be incorporated within holographic sensors by displaying a different image upon interacting with a target analyte.

Table 1. The quantification capabilities of holographic sensors in medical diagnostics

Stimulus	**Recognition Group**	**Dynamic Range**	**Sensitivity**	**Ref.**
Trypsin (μg ml^{-1})	Gelatin degradation	< 20	0.04	(Millington, Mayes, 1996)
Water content in solvents (ppm)	Matrix interaction	< 20,000	120	(Blyth, Millington, 1996)
Alcohol (%)	Matrix interaction	< 100	0.3	(Mayes et al. , 1999)
K^+ ions (mM)	18-crown-6	< 30	1	(Mayes, Blyth, 2002)
pH	Carboxylic acid	2-9	0.0006	(Marshall, Blyth, 2003, Tsangarides, Yetisen, 2014, Yetisen, Butt, 2014a)
Glucose (mM)	Phenylboro	< 375	0.09	(Domschke et al. , 2006, Horgan et

	nic acid			al. , 2006, Kabilan, Blyth, 2004, Kabilan, Marshall, 2005, Kraiskii et al. , 2010, Lee et al. , 2004a, Worsley et al. , 2007, Worsley et al. , 2008, Yang et al. , 2006, Yang et al. , 2008, Yetisen et al. , 2014d)
Ionic strength (mM)	Charged sulphonate and quaternary ammonium	< 500	0.08	(Marshall et al. , 2004b)
Penicillin G (mM)	Penicillinase	< 1-25	0.05	(Marshall et al. , 2004a)
Urea (mM)	Urease	< 50	0.15	(Marshall, Young, 2004a)
Ca^{2+} (μM)	iminodiacetic acid, nitrilotriacetic acid	<70	2.2	(Bhatta et al. , 2007, Gonzalez et al. , 2005)
Lactate (mM)	Phenylboronic acid	< 12	0.1	(Sartain et al. , 2006, 2008)
Calcium dipicolinate (mM)	Acid-soluble spore proteins	> 50	40	(Bhatta et al. , 2008)
Humidity (%, RH)	Matrix interaction	10-80	1	(Naydenova et al. , 2011, Naydenova, Jallapuram, 2008, 2009)
Edrophonium (μM)	Acetylcholinesterase and carboxylic acid	< 300	0.4	(Tan and Lowe, 2009)
Alkanes, alkenes, alkynes (% v/v)	Matrix interaction	< 100	0.5	(Martinez-Hurtado, Davidson, 2010, Martinez-Hurtado et al. , 2011)
Co^{3+} (mmol l^{-1})	Ionogens	< 10	0.1	(Kraiskii, Postnikov, 2010)
Organic solvents (%, v/v)	Matrix interaction	< 10	0.1	(Yetisen, Qasim, 2014g)
Testosterone (μM)	Molecular imprinting	< 10	1.0	(Fuchs et al. , 2014, Fuchs et al. , 2013)
Cu^{2+}, Fe^{2+} (1 M)	Porphyrins	< 1.0	0.1	(Yetisen, Qasim, 2014g)
Ammonia (NH_3) (%, v/v)	Nafion	0.19-12.5	2	(Hurtado and Lowe, 2014)
Pb^{2+}	8-Hydroxyquinoline	0.1-10.0 mM	11.4 μM	(Yetisen, Montelongo, 2015a)

1

2.2. Crystalline Colloidal Array Sensors

Periodic colloidal crystals based on microparticles can restrict the propagation of photons within a certain range of wavelengths – the photonic bandgap. In nature, such structures are found in opals, in which amorphous silica particles are periodically arranged. The optical characteristics of the diffracted light from colloidal crystals depend on the particle order, size, and the refractive index of the particles and their surrounding medium. CCAs embedded in hydrogels represent a colorimetric and reversible sensing technology for applications in IVD (Zhao, Zhao, 2010a). CCAs consist of three-dimensionally ordered polystyrene or poly(methyl methacrylate) (PMMA) nanoparticles that self-assemble into a body-centered cubic (BCC) or face-centered cubic (FCC) lattice due to electrostatic repulsion between the monodisperse, highly charged particles. With a mesoscopic periodicity of 0.1-1.0 μm, the CCA forms single crystals that Bragg-diffract visible light (Figure 2a) (Carlson and Asher, 1984, Rundquist et al. , 1989). The diffracted light is monochromatic and can be tuned in the visible spectrum (Figure 2b).

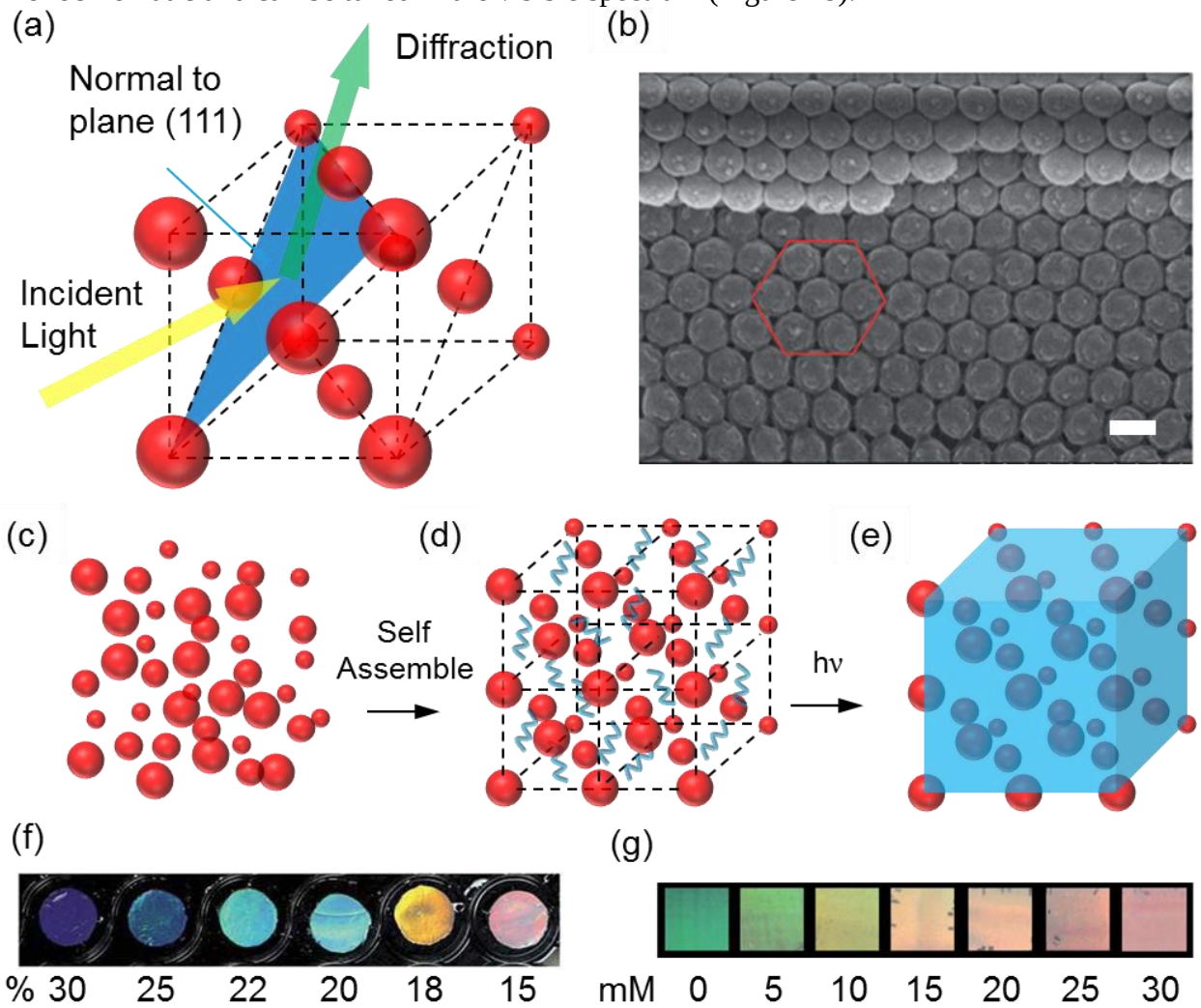

Figure 2. Crystalline colloidal array (CCA) sensor. (a) The principle of operation that obeys Bragg's law. (b) Scanning electron microscopy image of CCAs showing face centered cubic (FCC) array. Scale bar = 2 μm. Reprinted with permission from (Sai et al. , 2013) Copyright, the Royal Society of Chemistry. (c) Monodisperse, highly charged polystyrene or PMMA spheres synthesized through emulsion polymerization that (d) undergo electrostatic repulsion and self-

assemble to form FCC lattices, with subsequent (e) monomer mixture photopolymerized around the CCA (f) The diffracted light from CCAs can be tuned in the visible spectrum by changing the concentrations of the silica nanoparticles. Reprinted with permission from (Ye et al. , 2011) Copyright, American Chemical Society. (g) Colorimetric response of molecularly imprinted CCA sensors as the concentration of *p*-nitrophenol was increased from 0 to 30 mM. Reprinted with permission from (Xue et al. , 2014b) Copyright, The Royal Society of Chemistry

The synthesis of monodisperse, highly charged polystyrene or PMMA spheres (100 nm) can be achieved through emulsion polymerization (Reese et al. , 2000) (Figure 2c). A solution (~8 wt % colloids) was combined with a monomer mixture and allowed to equilibrate (Figure 2d). CCAs were then fabricated by the co-polymerization of monodisperse nanoparticles and monomers to immobilize the array suspension (Figure 2e) (Asher et al. , 1994). The CCA lattice spacing and subsequent diffracted wavelength depends on the concentration of the CAA and hydrogel volume. The diffracted light peak can be tuned by varying the concentration of the colloidal nanoparticle solution (Figure 2f). For example, a change of 0.5% in the hydrogel volume shifted the diffraction by ~1 nm (Holtz and Asher, 1997).

By incorporating different recognition sites, CCAs have been used for several applications in IVD. The CCA materials can be functionalized with chelating agents and ligands. Hydrogels consist of greater than 85% water, which allows target analytes to freely diffuse into the CCA matrix to bind to the recognition group with diffusion constants that can be approximated by those in water (Asher et al. , 2002). As the recognition group in the hydrogel matrix binds to target analytes, the Donnan osmotic pressure of the hydrogel matrix increases (or decreases) by absorbing more (or less) water. The changes the hydrogel volume is thus directly proportional to the concentration of the target analyte (Holtz and Asher, 1997, Holtz et al. , 1998). This volume change shifts the diffracted Bragg peak to longer wavelengths, which can be correlated with the analyte concentration. The color change can be semi-quantatively interpreted by eye, or quantitatively analyzed using a spectrophotometer. Therefore, CCAs offer a practical and equipment-free approach to IVD that can be used in the field to obtain rapid analyses.

The volume-phase transition of carboxylated CCA acrylamide-based hydrogels in response to pH and ionic strength changes has been monitored (Lee and Asher, 2000). The pH sensor operated from pH 2-11 and produced a ~250 nm shift in the Bragg peak. The shift due to Na^+ ions (10 mM) was 200 nm at pH 8.1. A volume-phase model was also developed to predict pH and ionic strength dependence of hydrogel swelling. This enabled the design of materials for optimal pH and ionic strength sensors by using functional groups that ionize in various pH ranges or that show no pH dependent ionization.

Crown ethers were attached to the polyacrylamide CCA hydrogel to selectively bind Pb^{2+} ions (Asher, Peteu, 2002). The measurement of blood lead concentration has diagnostic applicability in plumbism (lead poisoning). The reference range for acceptable blood lead concentration (BLC) is 0.5-1.0 µmol/L (Kratz, 2004). In lead poisoning, BLC exceeds 0.97 mmol/L (Haslam, 2003). Lead encephalopathy, more common in children than adults, is diagnosed at blood lead concentrations from 4.83-14.49 mmol/L (Trope et al. , 2001). The immobilization of Pb^{2+} ions in the CCA increased the influx of their counterions, which increased the Donnan osmotic pressure and swelled the hydrogel in proportion to the concentration of bound Pb^{2+} ions (Asher, Peteu, 2002). A red-shifted Bragg diffraction acted as a sensor for quantification of the concentration of Pb^{2+} ions in low ionic strength solutions. However, in high ionic strength solutions, the Donnan osmotic pressure from Pb^{2+} ion chelation

was saturated by non-specific interaction with other cations in the solution, and the sensors become ineffective. To overcome this challenge, the CCAs were incubated in a sample solution, and their transient response was measured after rinsing the sensor with pure water. Since the non-complexed counterions diffuse out of the CCA matrix more quickly than the bound Pb^{2+} ions, this transient diffraction shift was proportional to the concentration of Pb^{2+} ions. CCAs sensed Pb^{2+} ions in high ionic-strength environments such as body fluids with a detection limit of 100 ppb. For lead concentrations greater than 10 μM, the CCA color change was visible to the unaided eye. To detect lower concentrations of Pb^{2+} ions in high ionic strength, an optode sensing device was developed (Reese and Asher, 2003). This device consisted of a probe assembly containing the CCA sensing material, a diode array spectrometer, and a fiber optic reflectance probe. The optode might allow for the rapid removal of non-complexed ions present in biological samples. Recently, a CCA sensitive to thiocyanate ions (SCN^-) has been synthesized (Ma et al. , 2013). Polystyrene-co-poly(*N*,*N*-dimethylacrylamide) (PS-*co*-PDMAA) microspheres consisting of PS core and PDMAA shell have been prepared by emulsion polymerization (Xiao et al. , 2004). To construct the array, 3D self-assembly of a CCA was induced by centrifugation. Consequently, the CCA was tested in a plate groove. As the concentration of SCN^- ions increased from 8.6 to 860 nmol/g, the Bragg peak linearly red shifted 290 and 60 nm, respectively. The red shifts of other anions (8.6 nmol/g) were greater than 95 nm. While this assay provided broader operational wavelength ranges as compared to the polymerized CCAs, this assay required centrifugation for each experiment.

Polyacrylamide CCAs containing creatinine deiminase enzyme and 2-nitrophenol titrating group were used to detect and quantify creatinine, a marker of renal dysfunction, in human blood serum samples (Sharma et al. , 2004). When creatinine diffused into the hydrogel matrix, it became hydrolyzed by the creatinine deiminase enzyme, creating hydroxyl groups and increasing the local pH, which deprotonated a second recognition agent, 2-nitrophenol. The deprotonated phenolate exhibited enhanced solubility, swelled the hydrogel matrix and red shifted the Bragg peak. The changes in the Bragg peak position allowed the quantification of creatinine concentration with a physiologically relevant limit of 6 μM (Sharma, Jana, 2004).

Organophosphorus compounds are potent inhibitors of nervous system function and are used worldwide in agriculture, creating a need for a rapid, low-cost method of their detection (Dziri et al. , 1998, Radic et al. , 1993). The organophosphorus compound parathion was detected as low as fM using CCA sensors containing acetylcholinesterase (AChE) (Walker and Asher, 2005). AChE bound organophosphorus compounds irreversibly and created anionic phosphonyl species, which increased the Donnan osmotic pressure in the hydrogel matrix that red shifted the Bragg peak. Since the binding was irreversible, the AChE-CCAs acted as dosimeters for parathion.

Elevated concentrations of ammonia in the blood damages the central nervous system and inhibits the generation postsynaptic potentials (Hazell and Butterworth, 1999, Lockwood, 2004). Routine screening of ammonia blood concentration of at-risk patients is a clinical need that could prevent neurological damage. (Bachmann, 2003). Hyperammonemia is commonly associated with cirrhosis and chronic alcoholism, in which the liver cannot adequately clear out ammonia (Shimamoto et al. , 1999). An ammonia sensor that quantified the concentration of ammonia in human blood serum in the physiological range of 50-350 μM was synthesized by binding 3-aminophenol to the poly(hydroxyethyl acrylate) CCA backbone (Kimble et al. , 2006). Ammonia reacted with hypochlorite and the pendant aminophenol in the Berthelot reaction to create benzoquinone chlorimine, which reacted with another pendant aminophenol to form a crosslink.

The crosslinking of the hydrogel caused the matrix to shrink, and blue-shifted the diffracted light.

Recently, a CCA sensor has been developed to detect enzyme activity by tethering a target peptide (LRRASLG) to the hydrogel matrix as a substrate for protein kinase A (PKA) (MacConaghy et al. , 2015). The peptide became phosphorylated by PKA, resulting in additional negative charges in the hydrogel and the creation of a Donnan potential which changed the hydrogel volume and subsequently shifted the Bragg diffraction. By eliminating extraneous charges in the hydrogel through functionalization with azide-alkyne click chemistry, the hydrogels were able to detect phosphorylation in 30 min and had a sensitivity limit of 0.1 U/μL PKA in 2 h (MacConaghy, Chadly, 2015).

The diagnosis and treatment of diabetes also require rapid sensors that can be produced at low-cost. Phenyl boronic acid derivatives form reversible covalent bonds with carbohydrates through *cis*-diol binding (Hisamitsu et al. , 1997, Zhang et al. , 2013a). Boronic acid (pK_a = 8.8) is in uncharged and trigonal configuration below pH 7.0; however, at pH values greater than its pK_a value, boronic acid is in tetrahedral coordination form (Springsteen and Wang, 2002). The tetrahedral form can bind to *cis*-diol groups of carbohydrates, resulting in boronate ionization. This binding mechanism has been utilized in CCAs for sensing carbohydrates (Asher et al. , 2003). A CCA was synthesized from copolymerization of acrylamide and boronic acid derivatives. The sensor produced a Bragg peak shift of 60 nm as the concentration of glucose was increased to 10 mM (pH 8.5, 2 mM tris-HCl buffer). In another study, CCA embedded in phenyl boronic acid derivative functionalized polyacrylamide-poly(ethylene glycol), and a polyacrylamide-15-crown-5 matrixes were utilized to quantify the concentration of glucose in solutions (Alexeev et al. , 2003). The complexation of phenyl boronic acids and the *cis*-diol groups of glucose molecules increased the hydrogel crosslinking, and blue-shifted the Bragg peak. For example, a boronic acid-polyacrylamide- poly(ethylene glycol) CCA sensor produced a blue Bragg peak shift by 60 nm for 8 mM glucose (pH 8.5, 2 mM tris-HCl buffer) while the sensor produced a 100 nm shift at pH 9.5 (Figure 2g) (Alexeev, Sharma, 2003). Table 2 shows the dynamic ranges and sensitivities of various CCAs.

Table 2. Crystalline colloidal array sensors

Stimulus	**Recognition Group**	**Dynamic Range**	**Sensitivity**	**Ref.**
Pb^{2+} ions	18-crown-6	<7.5 mM	0.5 μmol/L	(Asher, Peteu, 2002)
Urea	Urease	0.05 mM – 0.5 mM	N/A	(Zeng et al. , 2002)
Glucose	Phenylboronic acid	< 30 mM	50 μM	(Asher, Alexeev, 2003, Zhang, Losego, 2013a)
Creatinine	Creatinine deiminase	<1 mM	0.01 mM	(Sharma, Jana, 2004)
Temperature	Poly(*N*-isopropylacrylamide)	25-40	N/A	(Lyon et al. , 2004)
Parathion	Acetylcholinesterase	<42.6 pM	4.26 fM	(Walker and Asher, 2005)
Ammonia	Berthelot reaction	50-300 μM	50 μM	(Kimble, Walker,

				2006)
Ethanol	N/A	< 100 % (v/v)	N/A	(Chen et al. , 2011)
Hg^{2+} ions	Urease-urea hydrolysis	< 20 ppb	1 ppb	(Arunbabu et al. , 2011)
Bisphenol A	Imprinted cavity	< 1 μg/mL	1 ng/mL	(Guo et al. , 2012)
pH	N/A	2.8-9.5 units	0.05 units	(Jiang et al. , 2012)
Cu^{2+}, Ni^{2+}, Zn^{2+} ions	8-hydroxyquinoline	<1.6 μM	0.08	(Jiang, Zhu, 2012)
Cd^{2+} ions	Thiourea	<10 mM	0.01 mM	(Lin and Yu, 2012)
Avidin	Biotin	1 mg/mL	580 nm/(mg mL^{-1})	(Zhang et al. , 2013b)
Diethylstilbestrol	Imprinted cavity	2 ng mL^{-1} - 8 μg mL^{-1}	N/A	(Sai, Ning, 2013)
Protein kinase A	Peptide LRRASLG	10 U/μL	0.1 U/μL	(MacConaghy, Chadly, 2015)

Molecularly imprinted polymers (MIPs), which have been used in chemical and biological sensors as selective recognition elements with a high affinity for the target molecule, can also be used to create defects in CCAs. MIPs contain specific recognition sites that are complementary in size, shape and functional groups to the template molecules and involve an interaction mechanism based on molecular recognition (Wulff, 1995). For example, CCA sensors incorporating MIPs were used for the detection of bisphenol A (BPA), a suspected endocrine-disruptor which adversely affects human growth and development (Guo, Zhou, 2012). Molecularly imprinted monodisperse PMMA nanoparticles were prepared with suspension polymerization, resulting in numerous nanocavities distributed in the PMMA spheres that provided specific recognition sites for BPA. By measuring the change in diffraction intensity corresponding to BPA concentrations, the sensor can detect between 1 ng/mL and 1 g/mL (Guo, Zhou, 2012). Similarly, the combination of molecular imprinting and CCA materials has also been used for the detection of diethylstilbestrol (DES), which has clinical utility in testing risk breast cancers and clear cell adenocarcinoma of the cervix (Palmer et al. , 2006, Sai, Ning, 2013). The diffraction intensity of the CCA decreased in 7 min upon increasing the DES concentration from 2 ng/mL to 8.2 mg/mL with no obvious changes in diffraction for DES analogues (Sai, Ning, 2013). Furthermore, molecularly imprinted CCAs have been used to measure the concentration of *p*-nitrophenol (Xue, Meng, 2014b). As the concentration of *p*-nitrophenol was increased to 30 mM, the Bragg peak of the CCA shifted 55 nm to longer wavelengths, showing a detection limit of 1 mM. The color change was visible to the eye (Figure 2g).

CCAs that can maintain their color independent of the observation angle have been synthesized (Yeo et al. , 2015). Monodisperse double emulsions encapsulating CCAs were prepared using a microfluidic device. Inducing crystallization of highly-charged polystyrene particles in the core of double emulsions through osmotic annealing allowed creating CCAs with improved angle tolerance. This approach also enabled tuning the shape and crystallinity of the CCA supraparticles. These supraparticles were subsequently were fixed in an elastomeric matrix. However, this approach produced broadband Bragg diffraction at low intensity, limiting the practicality for sensing applications. Recently, CCAs having uniform, Janus, multicomponent, or core-shell inner structures have been reported (Zhao et al. , 2014, Zhao et al. , 2010b). The

spherical symmetry of such "bead-shaped" CCAs enables their PBGs to be independent of the rotation angle under illumination of the surface at a fixed incident angle. Hydrogel DNA-responsive photonic beads were used for a label-free DNA detection (Zhao et al. , 2010c). The hybridization of target DNA and the crosslinked single-stranded DNA in the hydrogel grid causes hydrogel shrinking, leading to a blue shift in the Bragg diffraction peak.

Defects can be introduced to CCA as recognition sites by controlling the population and arrangement of nanoparticles through the creation of gaps, points, lines, planes, and grain boundaries (Arsenault et al. , 2006). Such defects allow engineered functionality for integrated optics applications. For example, creation of a single row of missing spheres to a CCA can provide a path for light guiding through the periodic lattice. Additionally, a bend can be created in the waveguide on the order of the wavelength of the light and a bend radius on the order of one particle diameter. This approach enables the creation of miniaturized circuit patterns that may find application in integrated optics and sensors. Defects in CCA can be introduced by photolithography, direct writing in confocal microscopy, and high-energy beam surface writing. Air core waveguides were constructed in silicon inverse opals by inserting linear air cavities in the interior of a lattice of silica spheres (Vekris et al. , 2005). This process involved photolithographically printing a pattern of photoresist lines on the colloidal surface, and then depositing silica spheres to cover the photoresist layer. Next, this layer was removed to create a pattern of linear air cavities in the CCA. Advanced projection lithography can achieve a resolution on the order of 250 nm. Direct writing by laser confocal microscopy involved infiltrating a CCA with a monomer solution, and then scanning the focal volume through the interior of the CCA to locally polymerize the monomer solution. The unpolymerized monomer solution is then removed from the system to leave a polymeric defect in the CCA (Lee et al. , 2002, Pruzinsky and Braun, 2005). Linear polymeric patterns with a linewidth on the order of 2 μm at a depth of 0.5 μm can be achieved. High-energy beam writing of linear patterns on the surfaces of CCAs have also been demonstrated (Tétreault et al. , 2006). This process involved direct writing of laser or e-beam across the surface of the CCA to selectively remove material or induce changes. For example, ion lasers were used to change the local recrystallization of amorphous Si to nanocrystalline Si. This process reduced the refractive index from 4.0 to 3.6. Furthermore, irradiation of PMMA spheres with e-beam cleaved bonds to cause solubility in an organic solvent (Ferrand et al. , 2003). Hence, the exposed materials can be removed in a development step to create structural changes.

Planar defects in CCAs can serve as optical dopants that decrease the intensity of Bragg peak at specific wavelengths associated with pseudogap frequencies. The wavelength of defect states within the pseudogap depends on the thickness of the dielectric slab, and its refractive index (Tétreault et al. , 2004). A 2D defect consisting of a monolayer of spheres sandwiched between two opal layers with different diameters were created by the Langmuir-Blodgett technique (Egen et al. , 2003, Massé et al. , 2006, Zhao et al. , 2003). Such defects have also been introduced by spin coating spheres or nanocrsytalline aggregates in CCAs (Pozas et al. , 2006). Furthermore, chemical vapor deposition (Palacios-Lidón et al. , 2004, Tétreault, Mihi, 2004) and polyelectrolyte multilayers (Fleischhaker et al. , 2005a) have also been used to introduce these defects. Polyelectrolyte multilayers can be incorporated in photonic crystals by layer-by-layer deposition or transferring the layer over the surface of the photonic structure by using a PDMS stamp, followed by growing a send layer of CCA on top of the embedded structural defect. These polyelectrolyte defect layers were functionalized with photochemically active azobenzene polyelectrolytes and redox-active polyferrocenylsilane (PFS) metallopolyelectrolytes. The

polyelectrolyte incorporating azobenzene can be actively modulated based on photochemical trans-cis isomerization and thermal backisomerization of the azo group (Fleischhaker, Arsenault, 2005a). The defect transmission state of the redox active polyferrocenylsilane was modulated by oxidizing and reducing the ferrocene units (Fleischhaker et al. , 2005b). The polyelectrolyte layers allow the incorporation of dyes, quantum dots, colloids, and biopolymers such as proteins and DNA (Schönhoff, 2003). For example, CCAs were designed with planar polyelectrolyte defects that incorporated DNA and polypeptides (Fleischhaker et al. , 2006). These sensors were used to monitor DNA conformational changes and the enantioselective intercalation of daunorubicin.

2.3. Inverse Opal Sensors

Inverse opals are constructed by templating monodisperse spheres, typically consisting of silica, polystyrene, PMMA, or block co-polymers (Aguirre et al. , 2010). Close-packed arrays from suspended particles can be obtained through centrifugation, sedimentation, vertical deposition, and physical confinement in hydrogels (Furumi et al. , 2010, Xia et al. , 2000). These close-packed arrays serve as a template that allows infiltration, and the spheres are removed from the medium by pyrolysis and etching (Figure 3). Inverse opals can be constructed in hydrogel matrixes that are functionalized with covalently linked chelating agents or ligands that can specifically bind to target analytes. Such interactions change the lattice spacing and the refractive index of the interstitial spaces and the hydrogel medium. The physical changes in the hydrogel matrix can be read through the diffracted or transmitted light.

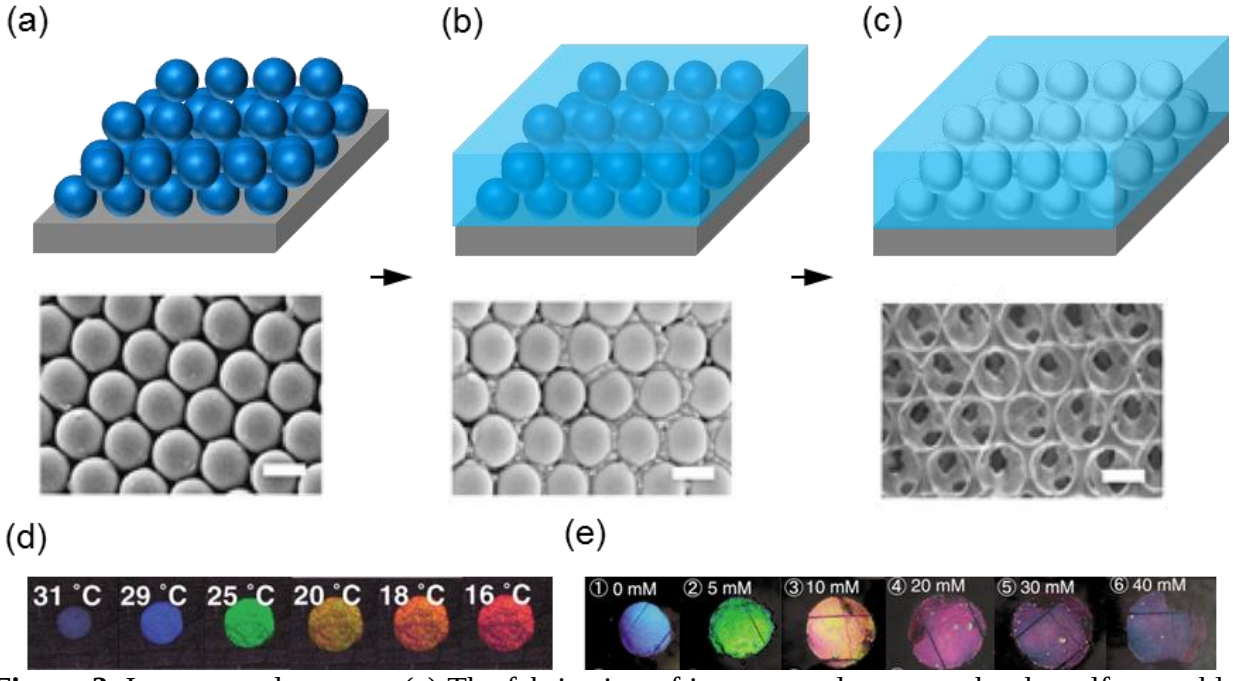

Figure 3. Inverse opal sensors. (a) The fabrication of inverse opal structure by the self-assembly of a colloidal crystal template, (b) infiltration by a monomer mixture, polymerization, and (c) the removal of colloidal crystal template, scale bars = 500 nm. Reprinted with permission from (Kim et al. , 2013), Copyright, Macmillan Publishers Ltd. (d) PNIPAAm-co-carboxylic acid thermosensors. Reprinted with permission from (Ueno et al. , 2007), Copyright, Wiley-VCH Verlag GmbH&Co. KGaA, Weinheim. (e) PNIPAAm-co-4-vinylbenzo-18-crown-6 K^+ ion

sensor. Reprinted with permission from (Saito et al. , 2003), Copyright, The Royal Society of Chemistry.

Inverse opals can be functionalized to be sensitive to external stimuli. Poly(*N*-isopropylacrylamide) (PNIPAAm) is a widely studied thermosensitive hydrogel that becomes hydrophobic at 32 °C by undergoing a phase transition from swollen to dehydrated state (Schild, 1992). An inverse opal PNIPAAm film was used as an optical filter by varying the temperature, which shifted the position of the Bragg peak and/or its intensity (Ueno, Matsubara, 2007). The thermosensor was prepared by copolymerizing *N*-isopropylacrylamide (NIPAAm), and methacrylic acid (MAAc). As the temperature was increased from 16 to 31 °C, the Bragg peak of the poly(NIPAAm-co-MAAc) matrix decreased from 660 to 340 nm (Figure 3d). The shift to shorter wavelengths originated from the shrinkage of the hydrogel matrix, which decreased the FCC lattice spacing. Another inverse opal temperature- and cation-sensitive sensor was templated from a silica sphere array by copolymerizing NIPAAm, *N*,*N*-methylenebisacrylamide, and 4-vinylbenzo-18-crown-6 (Saito, Takeoka, 2003). At 36 °C, K^+ ions (40 mM) shifted the Bragg peak by 200 nm to longer wavelengths (Figure 3e). However, the sensor was also sensitive to changes in the ionic strength of the cations. The color range of inverse opal hydrogels can be tuned by controlling the concentration of the crosslinker and the size of the templating spheres (Takeoka and Watanabe, 2003, Takeoka et al. , 2003). Humidity-sensitive inverse opal hydrogels were also developed using the hydrophilicity of polyacrylamide (Barry and Wiltzius, 2006). When the relative humidity was changed from 20 to 80%, the Bragg peak red shifted from 538 to 580 nm. Recently, humidity-sensitive silk-fibroin inverse opals were developed (Diao et al. , 2013). The humidity-induced cyclic contraction of silk fibroin enabled continuous modulation of the diffracted color. pH-sensitive inverse opal hydrogels were also synthesized from 2-hydroxyethyl methacrylate and acrylic acid (Lee and Braun, 2003). The range of Bragg peak shift can be controlled by changing the concentration of the acrylic acid and the crosslinker. The wavelength red shifted by 300 nm as the pH was increased from 4 to 7, showing a sensitivity of 0.01 pH units.

Inverse opals can be utilized as sensors for many clinically-relevant analytes. Glucose-sensitive inverse opals were synthesized in pHEMA matrixes containing 3-APB (Lee et al. , 2004b). Phenylboronic acid reversibly binds to 1,2-*cis* diols such as glucose, which increases the degree of ionization. This swells the hydrogel matrix by an influx of water and ions, and subsequently red shifts the Bragg peak. Inverse opals were optimized to respond to concentrations within the clinical range (<7.0-15.0 mM) of glucose in blood to indicate hyperglycemia (Nakayama et al. , 2003). The diffracted light shifted from green to yellow/orange to red as the concentration of glucose was changed from 5.0 to 10.0 to 15.0 mM. In another study, inverse opals were used to sense alcohols (Pan et al. , 2012). A single crystalline inverse opal hydrogel was fabricated by the polystyrene opal templating method in polyacrylamide. Its diffraction spectra changed from about 640 to 450 nm when the alcohol (methanol, ethanol, or *n*-propanol) concentration was increased. This sensor was also responsive to the variation in the concentration of polyethylene glycol. Inverse opals have also been used to detect ammonia (Liu et al. , 2012). TiO_2 inverse opals were fabricated by infiltration with polyaniline. The sensor changed its color from red to green reversibly in response to ammonia. This change was observed by eye, which may have clinical utility for monitoring ammonia vapor, such as from breath (Shimamoto, Hirata, 1999). Furthermore, dimethyl aminopropyl methacrylamide was incorporated in inverse opals as a functional monomer to sense CO_2 (Hong et al. , 2013). After

exposure to CO_2, the tertiary amine groups in this monomer were protonated and formed ion pairs with CO_2. This swelled the hydrogel matrix and red shifted the diffracted light. Non-invasive CO_2 sensors could have important implications for monitoring of respiratory physiology and pathologies (Folke et al. , 2003). Table 3 shows the inverse opal sensors and their detection capabilities.

Table 3. Inverse opal sensors and their detection capabilities

Stimulus	**Recognition Group**	**Dynamic Range**	**Sensitivity**	**Ref.**
pH	Carboxylic acid	2-7	0.01	(Lee and Braun, 2003, Xue et al. , 2014a)
Glucose	Phenylboronic acid	<100 mM	0.l mM	(Lee, Pruzinsky, 2004b, Nakayama, Takeoka, 2003)
Relative Humidity	Matrix interaction	20-80 %	1-10 %	(Barry and Wiltzius, 2006, Diao, Liu, 2013)
Temperature	Matrix interaction	16-31 ^{o}C	2 ^{o}C	(Ueno, Matsubara, 2007)
Bisphenol A	Molecular imprinting	10^{-8}-1 µM	10^{-9} µM	(Griffete et al. , 2012)
Cyanide	Trifluoroacetyl	<1 mM	10^{-4} mM	(Li et al. , 2012)
3-pyridinecarboxamide	Molecular imprinting	<10 wt %	0.5 wt %	(Yuan et al. , 2012)
PEG in 2-propanol	Matrix interaction	0-90 wt %	10 wt %	(Pan, Ma, 2012)
Ethanol, methanol, *n*-propanol	Matrix interaction	0-90 vol %	10 vol %	(Pan, Ma, 2012)
Ammonia	Polyaniline	1-4 (min)	30 nm/min	(Liu, Gao, 2012)
Glucose	Glucose oxidase	1-12 mM	0.5 mM	(Jin et al. , 2012)
Cholesterol	Molecular imprinting	1 nM - 10 µM	1 nM	(Zeng et al. , 2012)
Cu^{2+} ions	4-vinylpyridine	N/A	50 mM	(Hong et al. , 2012)
CO_2	Amino groups	0-4.9 vol%	1 vol%	(Hong, Chen, 2013)
Acetate	Thiourea	10 mM	1 mM	(Kado et al. , 2013)
Ammonia	Matrix interaction	< 100 vol %	N/A	(Zhong et al. , 2013)
Refractive Index	Gold nanoparticles	1.33-1.40	166 nm/RI unit	(Cai et al. , 2013)
Organic solvents	Matrix interaction	100 vol %	N/A	(Cui et al. , 2014)

Hg^{2+} ions	Carboxylic acid	10-1000 μM	10 nM	(Zhang et al. , 2014)
Avidin	Biotin	75-10000 nM	0.01 nm/nM	(Couturier et al. , 2015)

2D inverse opal hydrogels are promising candidates for sensing, and they have a number of advantages over traditional 3D inverse opal hydrogels (Li and Lotsch, 2012, Xue, Meng, 2014a). Their advantages include (i) faster and simpler formation of the 2D array template through self-assembly, (ii) a more stable ordering of the 2D array template, which makes it easier to introduce the pre-polymer solution into the template, and (iii) the optical characterization that can be achieved by analyzing Debye diffraction ring (Tikhonov et al. , 2012).

2.4. Porous Silicon Sensors

Photonic biosensors have been fabricated from porous silicon (DeLouise, Fauchet, 2005). A single crystal silicon wafer was electrochemically etched using hydrofluoric acid. The diameter (20-150 nm) and morphology of pores in n-type silicon were controlled by changing the etch parameters such as doping level, current density, and electrolytes. The resulting structures acted as Bragg gratings that can be tuned from visible to near-infrared regions of spectrum. Hydrogel-supported membranes were fabricated by either laminating the structure with a crosslinked hydrogel or pouring a monomer solution over the pores prior to crosslinking. Functionalizing the internal surface of the pores by bio-receptors and hydrogels allowed changing the position of the Bragg peak, which was correlated with concentration values of a target analyte. For example, polyacrylamide was functionalized with amine groups and incorporated into the porous silicon. Changes in the effective refractive index of disulfide crosslinked hydrogel in porous silicon were monitored upon exposure to tris(2-carboxyethyl) phosphine (TCEP). After submerging the photonic silicon in TCEP (50 mM) for 15 min and drying for 5 min, the reflectance peak shifted approximately 100 nm to shorter wavelengths (Bonanno and DeLouise, 2010). The color changes were visible to the eye. For detecting biomarkers in whole blood, amine-terminated porous silicon surface was functionalized with sulfosuccinimidyl-6-(biotinamido)-6-hexanamido hexanoate, and the sensor response was tested with biotinylated anti-rabbit IgG from goat (Bonanno and DeLouise, 2007). An increase in the concentration of IgG from 1 to 10 mg ml^{-1} produced ~3.3 nm wavelength shift. This approach offered intrinsic size-exclusion filtering of erythrocytes, which enhanced signal differentiation.

2.5. Block Copolymer Sensors

Block copolymers consist of two or more chemically distinct macromolecules that are joined together by covalent or non-covalent bonds (Kim, Park, 2010, Lynd et al. , 2008). A diblock copolymer consists of distinct polymers. The blocks can be linear chains of identical monomers or branched sequences of monomers. When the blocks are physically incompatible, different macromolecules are thermodynamically driven to self-assemble to reduce the contact between two immiscible regions (Fredrickson and Bates, 1996). Immiscible block copolymers undergo a microphase segregation to form nanostructures with dimensions ranging from 5 to 100 nm, and the control over this process allows tuning of their physical properties and morphology (Bockstaller et al. , 2005, Klinger et al. , 2013). Thermodynamically incompatible homopolymers phase separate to minimize the enthalpy of the system. However, in block copolymers, entropic forces from the covalent linkages counterbalance the thermodynamic forces driving separation

(Bates and Fredrickson, 2008). In contrast to the macrophase separation, the mobility of the copolymer is restricted locally due to the covalent bonding in block copolymers. Unfavorable monomer contacts and the tendency to minimize chain stretching locally segregate layers (Bockstaller, Mickiewicz, 2005). The phase behavior depends on three main factors: degree of polymerization (N), Flory-Huggins interaction parameter (χ), and the volume fraction of the block (Fredrickson and Bates, 1996). Using block copolymers, 2D/3D morphologies with different periodic lattice configurations can be achieved to create optical gratings (Bates and Fredrickson, 1990, Matsen and Bates, 1996). The polymer type, molecular weight, interaction parameter and processing conditions such as the degree of polymerization determines the morphology, such as lamellae, gyroid, cylindrical, or spherical (Figure 4a) (Hadziioannou and Skoulios, 1982).

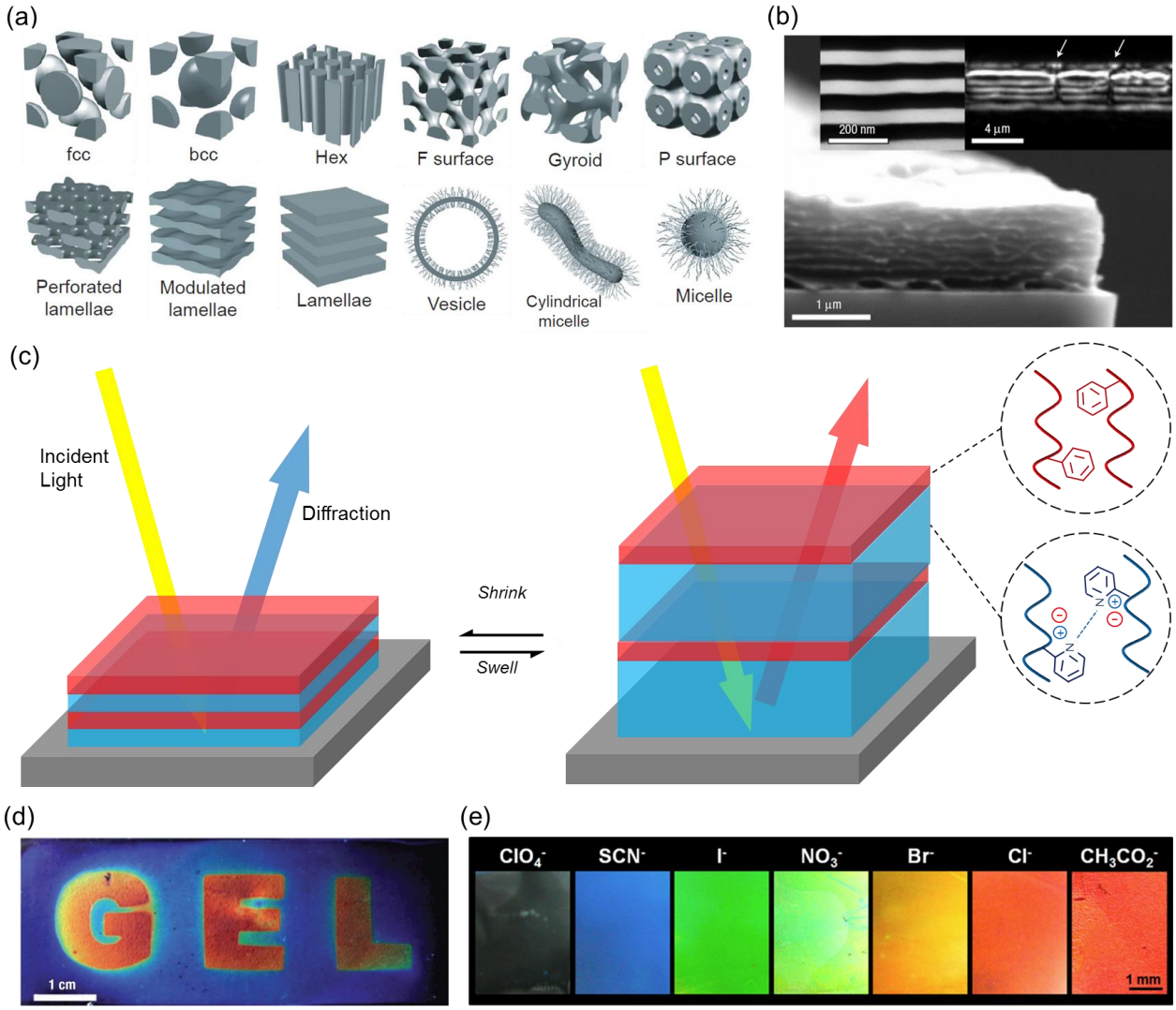

Figure 4. Block copolymer sensors. (a) Possible self-assembled architectures due to microphase separation. Reprinted with permission from (Bucknall and Anderson, 2003), Copyright, American Association for the Advancement of Science. (b) SEM micrograph of a polystyrene-*b*-quaternized poly(2-vinyl pyridine) block copolymer film deposited on a Si wafer. Reprinted with permission from (Kang et al. , 2007), Copyright, Macmillan Publishers Ltd. (c) The principle of

operation. The block-copolymer stack has alternating rigid layers (red) and dynamic polyelectrolyte layers (blue). (d) The degree of crosslinking allows tuning the diffracted light in aqueous solutions. Red regions have lower crosslinking density as compared to blue regions. Reprinted with permission from (Kang, Walish, 2007), Copyright, Macmillan Publishers Ltd. (e) Color change of the block copolymer films quaternized with direct exchange of counteranions. Reprinted with permission from (Lim et al. , 2012), Copyright, American Chemical Society.

Diblock copolymers have been used to construct Bragg gratings by solvent casting polystyrene-block-poly(ethylene/propylene) (PS-b-PE/P) (400 kg/mol) with a polymer dispersion index of 1.04 (Bockstaller et al. , 2001). This process created a periodic lamella structure with a spacing of 200 nm. When illuminated with a white light source, the Bragg grating diffracted light at 545 nm. Optical gratings can also be prepared by mixing diblock copolymers with its constituent homopolymers to swell the lamellar microdomains (Urbas et al. , 1999). The diblock copolymer/homopolymer allows tailorable lattice spacings, and the use of low molecular weight components. However, the production of optical gratings by self-assembly is limited due to incorrect size of domains needed for the optical ranges of interest, attainment of long-range order, and field of view, or cause low diffraction efficiency (Edrington et al. , 2001). The intrinsic dielectric contrast between the phases in block copolymer-based diffraction gratings is low, which limits the bandgap achievable by block copolymer-based Bragg gratings (Fink et al. , 1999). For example, the refractive index contrast between two phases of polystyrene-block-polyisoprene is 1.1. To improve the dielectric contrast, the microdomains of diblock copolymers can be doped with nanoparticles (Bockstaller, Kolb, 2001, Chiu et al. , 2005, Chiu et al. , 2007). The surface of nanoparticles can be functionalized to induce affinity to one of the phases of the block copolymer. For instance, PS-coated Au^0 nanoparticles with thiol-terminated ligands can be synthesized by the reduction of $HAuCl_4 \cdot 3H_2O$ in THF or two phase liquid system (Brust et al. , 1994, Yee et al. , 1999). Another challenge with diblock copolymers is that their absorption masks the diffraction within the visible spectrum. Hence, the practical short wavelength limit of diblock copolymers is ~300 nm since such systems have strong absorption in the UV region (Urbas et al. , 2002). Furthermore, self-assembled lamellae contain imperfections due to local phase separations and inconsistent orientation of the localized lamellar geometries in symmetric diblock copolymers (Edrington, Urbas, 2001).

The diblock copolymer gratings can be functionalized to render chemical-sensing capability. Polystyrene-*b*-quaternized poly(2-vinyl pyridine) (PS-*b*-QP2VP) lamellar films can be synthesized in a few steps. First, PS-*b*-QP2VP (5% wt, M_n = 190 kg mol^{-1}-*b*-190 kg mol^{-1}) in propylene glycol monomethyl ether acetate is spin-casted over a substrate, followed by annealing the matrix in chloroform vapor (50 °C, 24 h) to form in-plane oriented lamellar films (Kang, Walish, 2007). Subsequently, P2VP blocks were quaternized and crosslinked using a mixture of bromoethane and 1,4-dibromobutane (DBB) in hexane at (50 °C for 24 h). This process converted pyridine to pyridinium in the system. The resulting structure contained a microdomain periodicity of 100 nm with a matrix thickness of 1-3 μm (Figure 4b). When submerged into an aqueous solution, the polymer matrix expanded to 15-20 μm.

Block copolymers can consist of polystyrene-block-polyacrylic acid (PS-b-PAA), which consists of a hydrophobic PS block and pH sensitive hydrophilic PAA block. When illuminated with a white light source, block copolymer sensors operate through the modulation of their lattice spacing and, and hence shifting the Bragg peak to shorter or longer wavelengths (Figure 4c). The degree of swelling of the hydrogel matrix can be controlled by the density of

crosslinking. Highly-crosslinked regions of the block copolymer were blue and less-crosslinked regions were red in water (Figure 4d). This block copolymer matrix was used to non-specifically measure ionic strength in water (Kang, Walish, 2007). When different anions are introduced to the block copolymer matrix, the lamellar structure expanded or shrank depending on the hydration characteristics of each counterion (Lim, Lee, 2012). Another block copolymer matrix quaternized for 36 h with direct exchange of counteranions (10 mM) produced a color change in the visible spectrum (Figure 4e). In another study, temperature-sensitive block copolymers composed of high molecular weight poly(styrene-*b*-isoprene) (PS-*b*-PI) were anionically synthesized with styrene and isoprene monomers in cyclohexane and benzene (Yoon et al. , 2008). The resulting block copolymer matrix was sensitive to temperature changes (30-140 °C). Additionally, phenyl boronic acid derivatives were incorporated in block copolymers to sense carbohydrates (Ayyub et al. , 2013). PS-*b*-P2VP functionalized with 2-(bromomethyl)phenylboronic acid quantified the concentrations of fructose up to 50 mM with a detection limit of 0.5 mM. Although the self-assembly of block copolymers is a feasible method in creating multilayer Bragg gratings, it is limited by the requirement of synthesizing high molecular weight block copolymers for sensing applications.

The external shape and internal morphology of block copolymers (e.g., poly(styrene-block-4-vinylpyridine) (PS-*b*-P4VP)) have been controlled by positioning of Au nanoparticle surfactants to create convex particles (Ku et al. , 2014). The assembly of the Au NPs was localized at the interface between P4VP domain at the particles surface and the surrounding water. This created a balanced interfacial interaction between PS and P4VP domains of the block copolymer to form convex lenses.

2.6. Bragg Stack Sensors

Bragg stacks consist of alternating layers of high- and low-refractive index materials that upon interacting with incident light produce a strong coloration due to PBG. When the grating is illuminated with a white light source, the light is diffracted from each layer interface, creating narrow-band peaks. Such structures can be rationally designed by changing the film architecture, materials, and the periodicity to obtain desired optical characteristics. For example, the thickness can be varied by spin coating from 10 to 500 nm by controlling spinning speed, withdrawal rate, and the concentration of the deposited solution. Furthermore, the refractive index can be changed by modifying the composition of the deposited materials and the porosity. In bottom-up approaches, high- and low refractive index materials such as TiO_2 (n= ~2.85) and SiO_2 (n= ~1.44) can be used to construct multilayers (5-10). Many inorganic materials can be used to construct the Bragg stacks: metal oxides, zeolites, clays, metal-organic frameworks, metals, and semiconductors (Bonifacio et al. , 2009, Hinterholzinger et al. , 2012, Lotsch et al. , 2009).

Hydrogel-based Bragg stacks were constructed from a combination of TiO_2 nanoparticles, and hydrophobic and hydrophilic polymers such poly methyl methacrylate-co-2-hydroxyethyl methacrylate-co-ethylene glycol dimethacrylate (PMMA-*co*-pHEMA-*co*-PEGDMA) for application in sensing (Wang et al. , 2011). Figure 5a,b illustrates the principle of operation of Bragg stack sensors by increasing the thickness or changing the effective refractive index of the porous layer to induce a shift in the Bragg diffraction. In the presence of solvents, the Bragg peak shifted to longer wavelengths. The initial wavelength of Bragg stack sensors were tuned by changing the hydrogel-TiO_2 ratio during spin coating (Figure 5c-e). The Bragg stack sensors were tested in the presence of various organic solvents, where each solvent produced a different wavelength shift in the diffracted light (Figure 5f). For example, the shifts for ethanol and

DMSO were 60 and 420 nm, respectively. Another study reported a Bragg stack temperature sensor fabricated by coating high- and low- refractive index photo-crosslinkable copolymers: poly(paramethyl styrene) and PNIPAAm (Chiappelli and Hayward, 2012). As the temperature was increased from 20 to 50 °C in water, the Bragg peak blue shifted by 300 nm, producing a visible color change (Figure 5g). The fabrication of Bragg stacks with spin coating has a number of limitations. Spin coating is a multistep process consisting of drying and annealing steps between subsequent layers (von Freymann, Kitaev, 2013). Additionally, Bragg stacks are angle dependent; hence, their color changes are based on the position of observation (Bonifacio, Lotsch, 2009). The fabrication of organic-inorganic Bragg stacks is limited due to the instability of the polymer in the presence of inorganic sol (colloidal suspension). For example, the inorganic material solution containing TiO_2 sol is acidic, which distorts the morphological integrity of the sublayer (von Freymann, Kitaev, 2013).

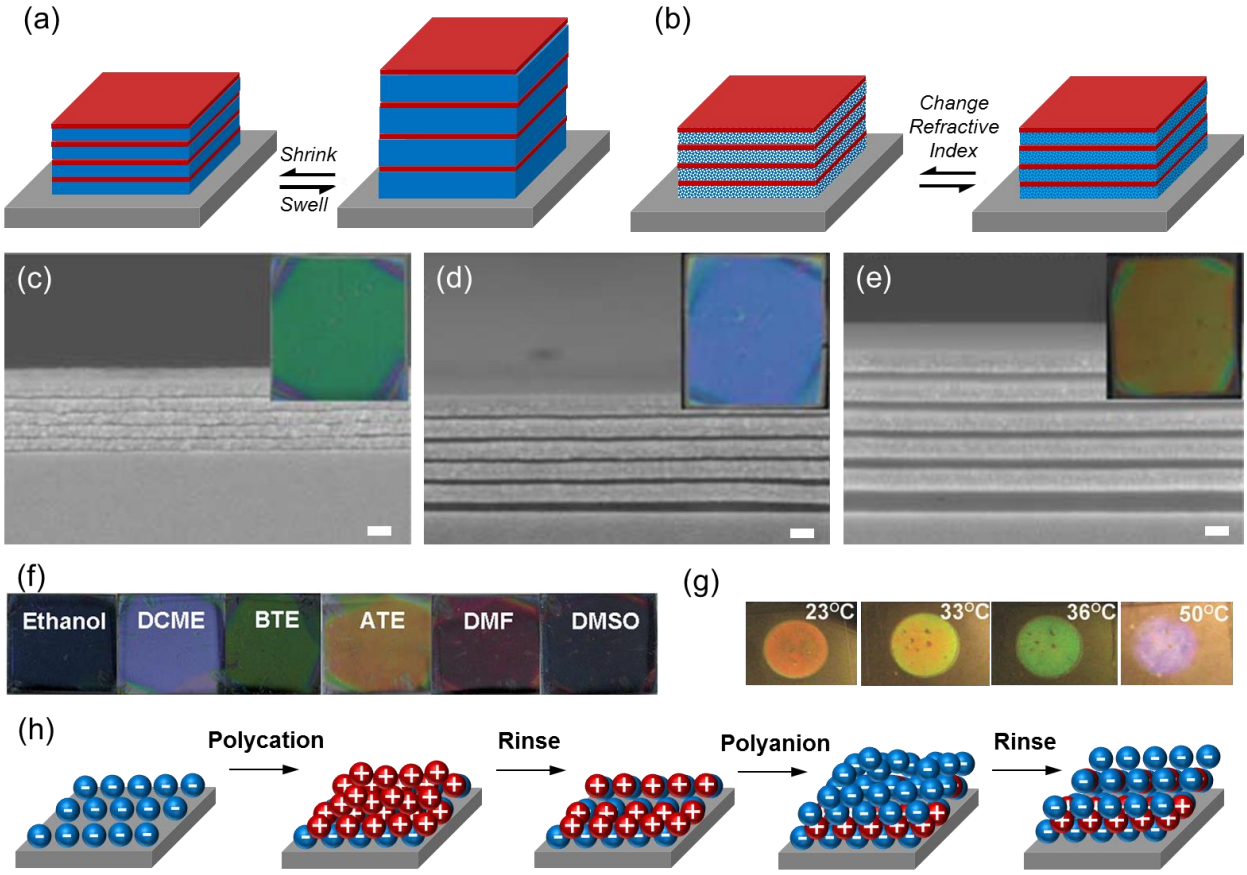

Figure 5. Bragg stack sensors. Principle of operation by (a) hydrogel swelling, and (b) Change of the effective refractive index. (c-e) SEM images of cross-sections of spincoated Bragg stacks consisting of TiO_2 and PMMA-co-pHEMA-co-PEGDMA with layer thicknesses of (c) 70 and 9 nm, (d) 80 and 20 nm, and (e) 89 and 57 nm. The insets show the diffraction at 2.0 × 2.0 cm. Scale bars = 100 nm. (f) The colorimetric response of spincoated Bragg stacks to organic solvents. (c-f) Reprinted with permission from (Wang, Zhang, 2011), Copyright, The Royal Society of Chemistry. (g) Colorimetric readouts of a poly(para-methyl styrene)-PNIPAAm Bragg stack temperature sensor in water. Reprinted with permission from (Chiappelli and Hayward, 2012), Copyright, Wiley-VCH Verlag GmbH&Co. KGaA, Weinheim. (h) Layer-by-

layer assembly of Bragg stack sensors through coating of polyanions and polycations on a negatively-charged substrate.

Layer-by-layer assembly is another approach to create Bragg gratings. It was first introduced for creating structured thin films in biotechnology applications (Decher et al. , 1992). The surfaces of many materials including glasses, silicons, and metals carry net negative charges in aqueous solutions due to surface oxidation and hydrolysis. When these planar or curved surfaces are immersed in positively charged polyelectrolyte solutions and rinsed with water, the net charge on the surface becomes positive since polyelectrolytes are absorbed and deposited over the negatively charged surface. Positively charged polyelectrolytes include poly(diallyldimethylammonium chloride) (PDDA), poly(allylamine hydrochloride) (PAH), and polyethyleneimine (PEI). Negatively charged polyelectrolyte solutions can be deposited over the positively charged polyelectrolyte layer, and these steps can be repeated until reaching a desired thickness (Figure 5h). The water rinsing step is required to remove unabsorbed polyelectrolytes from the surface. Negative polyelectrolytes include poly(styrene sulfonate) (PSS), poly(vinyl sulfate), or poly(acrylic acid) (PAA). This process builds alternating polyelectrolyte bilayers on the substrate. Layer-by-layer has an accuracy of 1 nm allowing nanoscale control of the thickness of films (Decher, 1997, Decher and Hong, 1991). While these self-assembly techniques are typically based on electrostatic interactions, polymer bilayers can also be constructed by using hydrogen and covalent bonding (Brynda and Houska, 1996, Sun et al. , 1998), hydrophobic interactions (Kotov, 1999, Lojou and Bianco, 2004), charge transfer (Shimazaki et al. , 1997), and biological recognition (Anzai et al. , 1999). In addition to polyelectrolytes, charged species of layer-by-layer bilayers may include carbon tubes (Jiang et al. , 2005, Mamedov et al. , 2002), nanoparticles (Kotov et al. , 1995), nanoplates (Keller et al. , 1994, Kleinfeld and Ferguson, 1994), organic dyes (Cooper et al. , 1995), porphyrins (Araki et al. , 1996), dendrimers (He et al. , 1999), polyoxometalates (Ingersoll et al. , 1994, Liu et al. , 2003), polysaccharides (Lvov et al. , 1998, Richert et al. , 2002), polypeptides (Boulmedais et al. , 2003, Müller, 2001), proteins (Hong et al. , 1993, Kong et al. , 1994, Lvov et al. , 1995, Lvov et al. , 1994), DNA and nucleic acids (Lvov et al. , 1993), and viruses (Yoo et al. , 2006). In sensing applications, poly(acrylic acid) (PAA)/poly(allylamine hydrochloride) (PAH) and PAA/poly(sodium 4-styrenesulfonate) (SPS) layers reversibly responded to pH and organic solvents (Zhai et al. , 2004). A significant limitation of layer-by-layer assembly is time consuming polyelectrolyte deposition, which take up to several hours.

3. Plasmonic Hydrogel Sensors

Localized surface plasmon resonance (LSPR) is an optical phenomenon in noble metal nanostructures involving sharp spectral absorption and scattering that allow them to be used as sensors. A plasmon refers to the oscillation of the free electrons in a noble metal (Mayer and Hafner, 2011). When the surface plasmons are optically excited, light is coupled into propagating or standing surface modes (Rochon and Lévesque, 2006). When a surface plasmon occurs around a nanoparticle sized on the order of the wavelength of the light, the free electrons produce a collective oscillation, which is called LSPR. This enhances the electric fields near nanoparticles' surface, and this effect decreases with distance. The optical extinction of the nanoparticle corresponds to a maximum at the plasmon resonant frequency. The extinction peak depends on the nanoparticle type and its complex refractive index (Mayer and Hafner, 2011).

The LSPR can be utilized in hydrogels to sense external stimuli based on the changes in the position of the peak wavelength or intensity. Figure 6a-d shows different configurations of plasmonic hydrogel sensors in thin films, array brush, core-shell colloids, and surface brush formats. Plasmonic nanoparticles can be incorporated in pH-responsive hydrogels. For example, gold nanoparticles were coated with pH-sensitive poly(methacrylic acid)-block-poly(*N*-isopropylacrylamide) (PMAA-*b*-PNIPAAm) (Nuopponen and Tenhu, 2007). In aqueous solutions, the nanoparticles aggregated as the pH was increased from 5 to 8. However, particle aggregation was irreversible. A blue shift in the LSPR was measured with decreasing pH or increasing temperature. Plasmonic crystal-based pH sensors were also reported (Mack et al. , 2007). First, a metallic fold film (50 nm) was coated over a square array consisting of 350 nm deep cylindrical impressions with 480 nm diameter. A monomer mixture consisting of hydroxyethyl methacrylate (HEMA), ethylene glycol dimethacrylate (EGDMA), acryclic acid (AA), and aqueous surfactant (Brij 58) was photopolymerized over the substrate. As the pH in the environment was increased, the hydrogel volumetrically expanded and decreased the refractive index. This shifted the LSPR peaks to shorter wavelengths. The sensor reversibly detected the changes within the pH range of 1.44-7.86, with a precision of 0.1 pH units.

Another study reported lithographically fabricated gold nanocrescents, which were coated with a pH-sensitive pHEMA hydrogel matrix (Jiang et al. , 2009). The LSPR of these nanocrescents operated in the near infrared region. As the pH was increased from pH 4.5 to 6.4, LSPR peaks shifted to shorter wavelengths, achieving an accuracy of 0.045 pH units. Plasmonic sensors based on polymer brushes were also synthesized (Tokareva et al. , 2004). Gold nanoparticles attached to poly(2-vinylpyridine) polymer brushes over gold nanoislands allowed reversible monitoring of pH changes by transmission spectroscopy. When the pH was changed from 5.0 to 2.0, the polymer brushes swelled from 8.1 to 24.0 nm. This volumetric change shifted the absorption maximum of the transmission SPR spectrum of the supporting gold nanoislands by 50 nm. Furthermore, light-controlled switching was demonstrated for Au nanorods encapsulated in the thermoresponsive PNIPAAm shells (Rodríguez-Fernández et al. , 2011). Au nanorod cores can be simultaneously used as fast optothermal manipulators (switchers) and sensitive optical reporters of the hydrogel state based on the analysis of the shifting behavior of the nanorod longitudinal plasmon.

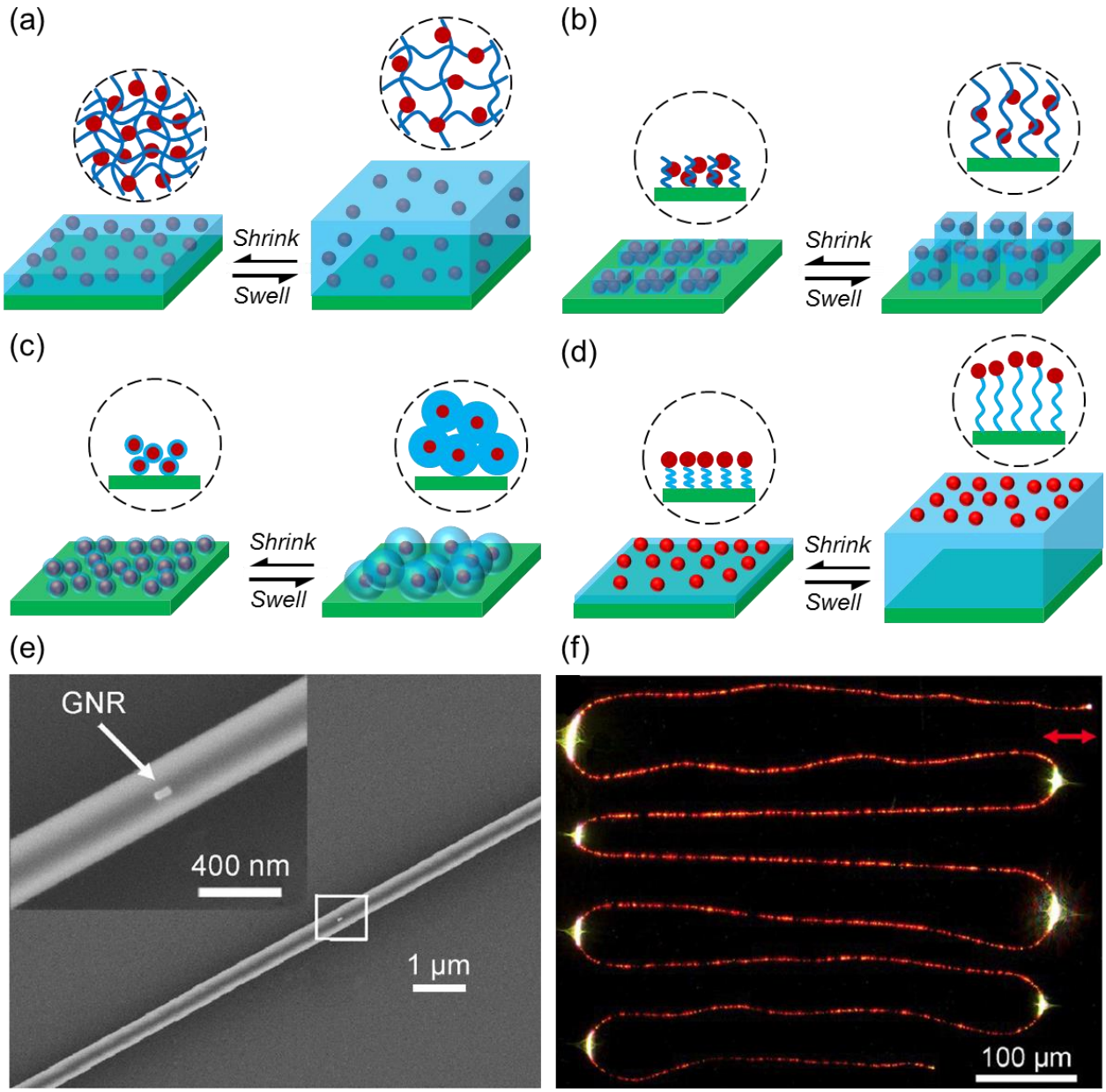

Figure 6. Plasmonic hydrogel sensors. (a) Thin film hydrogel containing plasmonic nanoparticles, (b) microhydrogel array brush containing plasmonic particles, (c) 2D/3D assembly of core-shell colloids, (d) surface immobilized nanoparticles on the surface of a hydrogel brush, showing their microscale and their polymer architectures. (e) An SEM image of a gold nanorod/polyacrylamide nanofiber (Ø=340 nm). The inset illustrates a magnified nanofiber where a gold nanorod was positioned. (f) Dark-field images of a gold nanorod embedded in a polyacrylamide nanofiber (Ø=440 nm, l=4.1 mm) at parallel polarization. The white spots at the bended sections show scattered light. (e,f) Reprinted with permission from (Wang et al. , 2012), Copyright, American Chemical Society.

Plasmonic hydrogel sensors were also used for measuring concanavalin A (Morokoshi et al. , 2004). Gold nanoparticles were functionalized with disulfide-carrying polymer with pendent glucose residues (poly(2-methacryloyloxyethyl d-glucopyranoside)). The binding of

concanavalin A to glucose was measured by LSPR sensing, showing a concentration-dependent response with a limit of detection of 1.9 nM. Another study reported the synthesis of DNA arrays using SPR hydrogel probes (Okumura et al. , 2005). DNA arrays were constructed by a surface modification technique for detecting K-*ras* point mutations, which is associated with the development of various malignancies such as lung and colon cancer. A homobifunctional alkane dithiol was adsorbed on the surface of a gold film to obtain a thiol surface and modified with ethylene glycol moiety, which supressed non-specific adsorption during SPR analyses. Steptavidin was immobilized on the modified surface, where biotinylated DNA ligands were attached to create DNA arrays. Finally, DNA probes conjugated with carboxylic acid-containing acrylamide nanospheres were bound to the target DNA in a sandwich configuration. The use of nanospheres produced an SPR signal enhancement and allowed the discrimination of a K-*ras* point mutation in the SPR difference image. Furthermore, polymer particles were doped with dyes to amplify the SPR signal originating from antibody-antigen interactions (Komatsu et al. , 2006). Such particles enhance the SPR signal by changing the imaginary part of the refractive index. The colorant improved the signal about 100 fold as compared to non-amplified SPR signal. Another study utilized dye-doped polymers and SPR allowed sensing Cu^{2+} ions (Ock et al. , 2001). The sensor consisted of a poly(vinylchloride)-poly(vinyl acetate)-poly(vinyl alcohol)copolymer film doped with squarylium dye and operated based on the changes in the refractive index upon interacting with Cu^{2+} ions. The sensor was sensitive to Cu^{2+} ions in buffer solutions at concentrations as low as 1 pM.

Plasmonic particles were coupled with MIPs to measure the concentration of cholesterol (Tokareva et al. , 2006). Gold nanoislands with a mean diameter of 14.5 nm were deposited over a glass substrate, where the interisland distance was 35 nm. These islands were spin coated over a 3 nm polyglycidylmethacrylate (PGMA) layer, which was used to graft carboxyl-terminated poly(2-vinylpyridine) (P2VP) over the substrate. Subsequently, gold nanoparticles (Ø=12 nm) and cholesterol were absorbed by the P2VP matrix and crosslinked by a quaternization reaction involving 1,4-diiodobutane to create the MIP layer. This MIP layer was used to sense cholesterol, where a 56 nm shift in the absorption maximum of the gold nanoislands was measured by T-SPR spectroscopy. MIPs were also utilized to detect domoic acid on a gold chip via SPR (Lotierzo et al. , 2004). Domoic acid is a marine neurotoxin that causes amnesic shellfish poisoning (Lelong et al. , 2012). A gold surface was functionalized with a self-assembled monolayer of 2-mercaptoethylamine, and 4,4′-azobis(cyanovaleric acid) was linked to the surface via carbodiimide chemistry. A 40 nm MIP film consisting of polymerized 2-(diethylamino) ethyl methacrylate and ethylene glycol dimethacrylate was attached to the functionalized surface. The resulting system enabled the use of a competitive binding assay to be performed with free domoic acid and its conjugate, while using horseradish peroxidase as a reactive label. The sensor allowed the measurement of domoic acid in buffer solutions through SPR readouts, achieving a detection limit of 5 ng/mL. Table 4 shows the plasmonic hydrogel sensors and their sensitivities.

Recently, newer platforms have emerged for utilizing SPR as the sensing probe. For example, polymer nanofibers consisting of aligned gold nanorods were utilized for sensing humidity (Figure 6e) (Wang, Zhang, 2012). A gold nanorod-doped polyacrylamide nanofiber at parallel polarization showed red scattered light (Figure 6f). The 540 nm thick nanofiber waveguides were illuminated at 785 nm from one end, and the intensity of the light output was measured from the other end. The scattering intensity of the waveguide decreased as the RH was increased. The sensor had a photon-to-plasmon conversion efficiency of 70% at its longitudinal

resonance wavelength, and it allowed quantifying relative humidity (10-70 %) within 110 ms using 500 pW at 785 nm.

Table 4. Plasmonic sensors and their applications in medical diagnostics

Stimulus	**Recognition Group**	**Dynamic Range**	**Sensitivity**	**Ref.**
pH	Carboxylic acid	3-12 units	12.5-19.5 nm/pH	(Mishra and Gupta, 2013, Singh and Gupta, 2012)
Glucose	Phenylboronic acid	< 50 mM	50 μM	(Mesch et al. , 2015)
Melamine	Gold nanoparticles	1 μg/mL	1 μM	(Manikas et al. , 2014)
Concanavalin A	Molecular imprinting	1 μM	0.5° Resonance angle shift/min	(Kuriu et al. , 2014)
Protein (FKBP12)	Carboxylated dextran	<10 nM	0.5 nM	(Li et al. , 2015a)
Trinitrotoluene	Molecular imprinting	83-250 μM	50 μM	(Cennamo et al. , 2013)
3-Pyridinecarboxamide	Molecular imprinting	0-10 mg/ml	1.483 nm/(mg/ml)	(Verma and Gupta, 2013)
Bisphenol A	Molecular imprinting	< 0.5 mg/dL	0.05 mg/dL	(Taguchi et al. , 2012)
4-mercapto-benzoic acid	Matrix interaction	$10\text{-}10^4$ nM	65 pM	(Ouyang et al. , 2015)
2,2-dipyridyl	Matrix interaction	$10\text{-}10^4$ nM	6.4 nM	(Ouyang, Zhu, 2015)
Water content in ethanol	Matrix interaction	< 10 vol %	0.5 vol %	(Mishra and Gupta, 2014)

4. Reflection and Refractive Index Modulation-Based Hydrogel Sensors

Changes in the refractive index can be used as a measurement mechanism in hydrogel matrixes that can dynamically respond to a target analyte. For example, hydrogel microlenses were utilized as optical sensors due to changes in the refractive index or radius of curvature (Ehrick et al. , 2007). The response due to swelling can be quantified by measuring the focusing power of the microlens (Figure 7a, b). When a hydrogel lens interacts with a target analyte, the degree of de/focusing of the lens can be correlated with the concentration. The microdome patterned hydrogels were synthesized by UV or thermally initiated free-radical polymerization over a glass substrate. The hydrogel microdome was synthesized from acrylamide copolymerized with calmodulin and phenothiazine derivatives. In the presence of the competing ligand chlorpromazine, calmodulin displaced phenothiazine, causing decrosslinking and gel swelling. This swelling changed the curvature of the microdome and its refractive index, defocusing the image. Microlenses were also constructed from hydrogel rings to control the curvature of a water-oil interface (Dong et al. , 2006). These rings were created from PNIPAAm and

functionalized with acrylic acid to create sensitivity for temperature and pH, respectively. The microlenses were produced by sandwiching a hydrogel ring between a glass surface and a hole, where the water was added, and oil was confined in this space. This produced a system with a water-oil interface at the center of the hydrogel ring. The curvature of the interface was modulated by volumetrically changing the hydrogel matrix through pH or temperature.

Another study reported the synthesis of thermosensitive PNIPAAm-co-acrylic acid microgels on aminopropyltrimethoxysilane (APTMS) functionalized glass substrates (Serpe et al. , 2004). Elecrostatic interactions allowed amine groups on the substrate to bind to the acrylic acid functionalized microgels. Upon attachment to the substrate and drying, the microgels deformed isotropically. The microgel curvature was modulated by changing the temperature, pH and solvents. The resulting structures were used as dynamically tunable lensing structures through the modulation of the size, focal length, and the refractive index (Kim et al. , 2004). Furthermore, these microlenses can be tuned with laser light. First, a glass substrate was doped with Au^0 nanoparticles (Ø=16 nm), and a cationic polyelectrolyte poly(allylamine hydrochloride) (PAH) was deposited on this surface to render it positively charged (Kim et al. , 2005b). PNIPAAm-co-AAc microgels were added to this system by adding it dropwise over the surface in a spatial manner. The resulting lens was excited at frequency-doubled Nd:YAG laser (λ= 532 nm) due to the plasmon modes on the Au^0 nanoparticles. Based on the same principle, microlenses that display refractive index changes were designed for protein sensing (Kim et al. , 2005a, Kim et al. , 2006, Kim et al. , 2007a, Kim et al. , 2007b). These microlenses consisted of binding- and displacement-induced formats. Vitamin biotin was conjugated to acrylic acid within the microlens, and the assay was tested in the presence of avidin or anti-biotin (antibody). The presence of avidin and anti-biotin increased the surface crosslinking of the microlens, which induced a refractive index change. Using an inverted microscope, a single square projection transited to double image in projection mode.

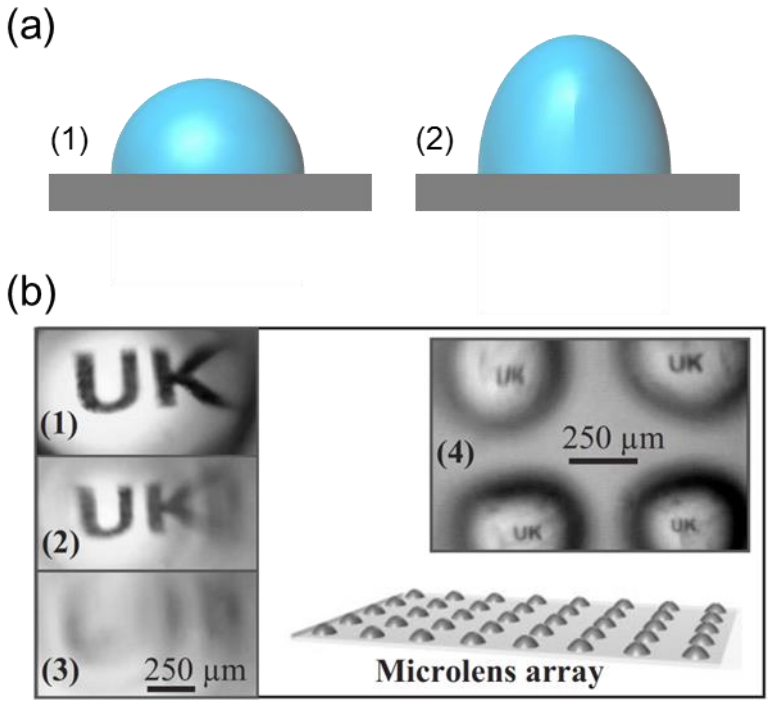

Figure 7. Reflection and refractive index based hydrogel sensors. (a) A schematic of a tunable hydrogel microlens in (1) the initial state and (2) swollen in the presence of an analyte. (b) Image focused through a polyacrylamide microlens in (1) the swollen state and (2, 3) defocused in a less swollen state. (4) The microlens array format. Reprinted with permission from (Ehrick, Stokes, 2007), Copyright, Wiley-VCH Verlag GmbH&Co. KGaA, Weinheim.

A layer of functionalized microgels has been sandwiched between two gold films to produce an etalon. Upon interacting with an analyte, functionalized microgels produced volumetric changes, resulting in visual color changes and shifts in multipeak reflectance spectra. The positions of the peaks in the spectra primarily depended on the distance between the gold layers mediated by the microgel thickness. Reductant-sensitive PNIPAAm microgels crosslinked with *N*,*N*'-bis(acryloyl)cystamine have been synthesized and incorporated in an etalon (Li et al. , 2015b). This device produced an optical response in the presence of dithiothreitol due to decrosslinking of the microgel matrix. The reflection peak of the etalon shifted ~45 nm as the concentration of dithiothreitol was increased from 0.19 to 1.50 mg/mL. Etalons were also used to sense ethanol (Huang and Serpe, 2015). As the concentration of ethanol was increased to 12 vol %, the reflectance peak shifted 60 nm to longer wavelengths. In another study, etalons were constructed from poly(*N*-isopropylacrylamide-co-*N*-(3- aminopropyl) methacrylamide hydrochloride) (pNIPAm-co-APMAH) microparticles, which were functionalized to be sensitive to negatively charged single stranded DNA (ssDNA) (Islam and Serpe, 2014). In the presence of target DNA (80 μM, pH 7.2), the reflectance peak shifted 60 nm to shorter wavelengths. Etalons constructed from pyridine-functionalized PNIPAAm have been used for gas sensing (Zhang et al. , 2015). As the CO_2 was introduced to the etalon, the reflectance peak shifted ~35 nm. A challenge in using etalons is that the readouts are broadband, which may limit colorimetric measurements by eye. Nevertheless, as compared to the other sensing approaches, etalons are easier to fabricate.

Analytes can also be sensed by a polymer-coated optical fiber tip. Optical fibers have several advantages such as remote sensing over long distances, small size and immunity to electromagnetic interference as compared to electrochemical sensors. The change in refractive index and swelling can be read out by measuring the reflectance or by an interferometric setup. In one embodiment, a pH sensor was created by dip coating a fiber with Kraton (61652), which was a styrene-ethylene, butylene-styrene, and a triblock copolymer (Shakhsher et al. , 1994). In its non-swollen state the polymer was opaque, but when the pH was decreased from 8.0 to 6.5, the amine groups were protonated; hence, the polymer swelled and became transparent. The change in refractive index and clarity decreased the intensity of the reflected light by a factor of 2. To improve the sensitivity to the changes in refractive index, an interference method was used (Wei Chang et al. , 2012). The fiber could be bitapered or a core offset could be introduced so that part of the core mode leaked into the cladding layer. Both core and cladding modes were reflected back from the coated fiber tip and were recombined in the fiber core. The optical path length difference between the two modes resulted in an interference pattern. The interference was measured by using a tunable laser as a light source and recording the output intensity as a function of its wavelength. Refractive index change was proportional to the wavelength shift of the interference. In one study, a bitapered optical fiber was coated with polyvinyl alcohol/poly-acrylic acid hydrogel. A pH sensitivity of 1.58 nm/pH was achieved in the pH range of 2.48–6.47 (Wong et al. , 2014).

Swellable polymer spheres dispersed in hydrogels can also be used as sensors. Such dispersions are optically opaque because of the mismatch of the refractive index of the spheres and the hydrogel, causing light scattering. Upon introduction of an analyte, the polymer particles change refractive index, scattering, and turbidity. The polymer microsphere method has advantages over surface immobilized polymers since the polymer is free to swell in all directions in the hydrogel matrix, eliminating the problems of deformation, cracking and detachment of the polymer layer. Furthermore, light transmission can be measured at any wavelength with different standard equipment such as a UV/Vis/NIR spectrometer. For example, a pH sensor has been made of a dispersion of aminated poly(vinylbenzyl chloride) microspheres (Ø=1 μm) suspended in a pHEMA matrix (Rooney and Seitz, 1999). Turbidity was measured when pH was changed from pH 4.0 to 10.0. In another study, pH-sensitive polymer particles were synthesized from *N*-isopropylacrylamide (NIPA) copolymerized with a crosslinker and pH sensitive functional comonomer and embedded in a PVA hydrogel matrix (Lavine et al. , 2012).

5. Tests in Biological and Clinical Samples

Photonic hydrogel sensors have been tested in blood and urine samples to analyze the interference from other analyte species. Holographic sensors containing phenylboronic acid (12 mol%), and trimethylammonium chloride (12 mol%) have been used to measure the concentration of glucose (3-33 mmol L^{-1}) in seven human blood plasma samples (Worsley, Tourniaire, 2007). Trimethylammonium chloride increased the sensitivity of phenylboronic acid to glucose over other saccharides possessing *cis*-1,2- or -1,3-diols (Horgan, Marshall, 2006). Experimental setup allowed varying the concentration of glucose from 0.17 to 0.28 mmol L^{-1} min^{-1} using glucose stock solution (44 mmol L^{-1}). The measurements were calibrated with an electrochemical analyzer (2300 STAT Plus). As the concentration of glucose was increased from 3.8 mmol L^{-1} to 30.9 mmol L^{-1}, the Bragg peak shifted from 640 to 571 nm. The reproducibility and repeatability of the holographic sensors ranged from 1.9-5.4 and 1.1-4.8, respectively. However, this approach required buffering the sample using sodium phosphate to keep pH constant at 7.4. Holographic sensors were also tested with urine samples of diabetic patients (Yetisen, Montelongo, 2014d). These sensors containing 3-APB (20 mol%) responded to glucose concentrations (2-10 mM) by changing their color from green to red. In clinical tests, the sensors were able to measure glucose up to 400 mmol L^{-1} within 3 min with a detection limit of 90 μM. A significant challenge with the readouts of phenylboronic acid is that *cis*-diol binding with glucose requires ~1-2 h to reach saturation. To shorten the response time, an algorithm was developed to correlate the concentration of glucose with the binding rate, and the readouts were achieved in 3 min. However, the interaction of 3-APB with glucose was pH dependent; hence, the measurements were conducted under fixed pH conditions.

Ammonia-sensitive CCAs have been tested with human blood serum (Kimble, Walker, 2006). This photonic crystal array included covalently attached 3-aminophenol to the poly(hydroxyethyl acrylate) matrix, which formed crosslinks through Berthelot mechanism. First, ammonia present in a solution reacted with hypochlorite to form a monochloramine, which in turn reacted with pendant 3-aminophenols to create a crosslink in the hydrogel matrix. pK_a values of 3-aminophenol are 4.37 and 9.81 for the amine and hydroxy functional groups, respectively. The crosslink formation in the hydrogel shifted the diffracted light to shorter wavelengths in proportion to the amount of ammonia present in the solution. The sensors tested in diluted human blood serum in borate buffer (pH 9, 50 mmol L^{-1}) showed Bragg peak shifts of 2, 4, 7, and 13 nm in the presence of 30, 75, 150, and 300 μmol L^{-1} ammonia within 1 h,

respectively. The detection limit of this sensor was 50 μmol L^{-1} (Kimble, Walker, 2006). A disadvantage of this sensor was that the samples required highly basic buffers to function. Furthermore, CCAs functionalized with 8-hydroxyquinoline have been used to measure Ni^{2+} ions in human plasma at neutral pH (Baca et al. , 2008). Polyacrylamide matrix containing CCAs was first hydrolyzed at 24 °C for 2 h. 1-ethyl-3-(3-dimethylaminopropyl)carbodiimide (EDC)-initiated reaction was used to covalently link 5-amino-8-hydroxyquinoline to the polyacrylamide matrix. When human plasma (10 mL) was added to $NiCl_2$ (0.75 mmol L^{-1}, 20 mL) in HEPES (pH 7.4, 50 mmol L^{-1}) buffer and NaCl (150 mmol L^{-1}), the Bragg peak of the sensor shifted to shorter wavelengths by 12.4 nm. This Ni^{2+} sensor had a sensitivity of 60 μmol L^{-1} (Baca, Finegold, 2008). However, blood plasma has a complex composition containing proteins and ions that contract the polyacrylamide matrix due to a decrease in Donnan osmotic pressure.

Porous silicon sensors were tested in opiate spiked human urine samples (n=50) (Bonanno et al. , 2010). The porous silicon was functionalized with an opiate-analogue (MG3). This was achieved via carbodiimide chemistry by linking MG3 to lysine groups present on a bovine serum albumin blocked surface. In oxycodone-free urine samples, monoclonal mouse antimorphine antibody (α-M Ab) bound to the opiate-analogue attached to silicon pore surface, which resulted in a 6 nm Bragg peak shift to longer wavelengths. Free opiates in urine competed for binding sites on the α-M Ab, and this resulted in a corresponding decrease in the wavelength shift. Limitations of porous silicon sensors include variation in the pore diameters of silicon, and wavelength shifts below 10 nm that are not possible to identify with eye.

6. Future Directions

Many bottom-up fabrication methods including layer-by-layer assembly, and spin and dip coating require the deposition of nanoparticle and polymer bilayers with high accuracy. In these approaches, the accuracy of the assembly depends on the sequential coating steps, which are time consuming. Faster deposition schemes might be achieved through automation and 3D printing (Xing et al. , 2015). For example, robotic coaters have been utilized in the spray layer-by-layer assembly of polyelectrolytes and TiO_2 and SiO_2 multilayers (Nogueira et al. , 2011). Such methods can achieve assembly faster than the immersion layer-by-layer assembly. Increasing the control of deposition parameters such as temperature, spinning and withdrawal times, the quantity and the concentration of solutions through robotics will allow creating uniform optical properties in centimeter-sized substrates. The broader use of ink-jet type material deposition systems will enable precise localization of the analyte sensitive species and the production of patterned gratings. Such devices may have the ability to convey a message at the moment of analyte detection. Furthermore, these approaches can include novel materials such as graphene, carbon nanotubes, quantum dots, magnetic nanoparticles, silk, nanofibers, nanocrystals, latex particles, and negative refractive index structures (Butt et al. , 2015, Deng et al. , 2014, Kong et al. , 2014, Kong et al. , 2015).

In visually read optical sensors, a significant limitation is the visibility of the photonic structures from wide angles. The semi-quantitative readout of photonic hydrogel sensors by eye is challenging. For example, in Bragg reflectors, the color of the diffracted light might depend on the position of the observer. Furthermore, as the hydrogel swells and shrinks, the angle of the diffracted light from the normal to the surface plane changes; this is an inherent property of Bragg reflectors. A significant contribution to the area would be the development of omnidirectional gratings that can be fabricated with high refractive-index contrast constituent layers. The incorporation of diffusers, lenses, reflectors, or other optical devices in photonic

gratings will improve the angle of view (Zhao et al. , 2015b). Some of these fabrication approaches may be inspired from structural color designs in nature (Oh et al. , 2014). However, such additional devices will decrease the intensity of the diffracted light in any given direction. Hence, the optimization of Bragg stack layers or the concentration of plasmonic nanomaterials in the hydrogel matrix will increase the diffraction efficiency of photonic sensors. Additionally, the development of algorithms that can estimate the position of the Bragg peak as the hydrogel matrix swells or shrinks will be a valuable contribution. Another potential area of development is tuning the sensors to operate in the entire visible spectrum; currently, only a few sensors have utilized broad colorimetric regions.

Photonic hydrogel sensors have high sensitivity ranging from pM to mM. However, a limiting factor for realizing the full potential of photonic hydrogel sensors is selectivity. Ionic strength, pH and temperature significantly affect the performance of these sensors. However, photonic hydrogels may be multiplexed to improve the dynamic range and obtain readouts from different sensors. Moreover, the integration of photonic hydrogel sensors with PDMS or paper-based microfluidics may allow multiplexing (Volpatti and Yetisen, 2014, Yetisen, 2015g, Yetisen and Volpatti, 2014). Such assays enable the use of low-volumes of fluids to carry out sample preparation for high-throughput analyses (Choi and Cunningham, 2007, Kim et al. , 2014). Additionally, testing the effects of batch-to-batch variability, oxidation, material decay, and long-term storage can be significant contributions in creating robust sensors. The fabrication techniques that allow constructing sensors from microporous hydrogels are required to increase the diffusion rates. For example, fabrication of photonic structures utilizing zeolite nanoparticles could be a feasible method to increase the response time of the sensors. Furthermore, the development of affinity ligands to control the specificity of targeting by antibodies and bioactive macromolecules such as nucleic acids and whole cells will be important contributions to the field. Additionally, while the hydrogel sensors that do not selectively bind to analytes had fast response times, the sensors with ligands take inherently longer times to bind to target analytes and reach equilibrium. This remains a significant issue as compared to other sensing mechanisms such as electrochemical sensing. Investigations in binding kinetics of chelating agents and ligands, and reversibility will enable the development of photonic hydrogel sensors with improved control over selectivity in addition to rapid response time. Studies in shrinking/swelling dynamics, non-specific interactions with hydrogel matrixes, surface energy and charge, hydrophilicity/phobicity, surface roughness, and polymer porosity will allow the rational design of sensors. Furthermore, the models that can simulate the properties of material during swelling and shrinking cycles, change in effective refractive index, plasmonic effects, diffraction and absorption spectra of the grating or the nanoparticles/dopants will contribute to the theoretical understanding of photonic hydrogel sensors.

The readout technologies of photonic hydrogel sensors should also evolve. Smartphone technologies have recently emerged as a platform to quantify the sensor readouts while offering connectivity options (Yetisen et al. , 2014b, Yetisen et al. , 2014c). This platform will also enable the real time reporting of the results of IVD testing. For example, readouts of photonic hydrogel sensors with tablet computers, smartphones/watches, or other wearable technologies can improve the existing user interface. The embedded light sources in these mobile devices may be utilized to standardize the illumination of the sensors. Such platforms also provide data processing to mitigate the interference from background noise of the sample or ambient light. While these readout technologies are required for quantitative analyses, there is also a significant market need for equipment free semi-quantitative diagnostics, where photonic hydrogel sensors may offer

solutions through their colorimetric readouts. Such devices may also include user-friendly fool-proof text or image reporting capabilities. Additionally, photonic hydrogels are not limited to IVD, but also offer possibilities in implantable chips (Choi et al. , 2013) and contact lens sensors (Farandos et al. , 2015), where long-term operation, biocompatibility are required for continuous quantification of analytes *in vivo*.

7. Conclusions

Many top-down and bottom-up approaches including laser writing, self-assembly and layer-by-layer deposition have been demonstrated to create Bragg diffraction gratings, microlenses, etalons and plasmonic structures in hydrogels. These hydrogels have been functionalized to be sensitive to a wide range of analytes by creating covalently-bound pendant recognition groups or molecularly imprinted sites. Utilizing the nanoscale structures as transducers, functionalized hydrogel matrixes have been utilized to quantitatively report on the concentrations of target analytes. When these sensors output narrow-band light over broad wavelength ranges in the visible spectrum, the readouts were visible to the eye for semi-quantitative analyses. Fully-quantitative readouts were obtained using spectrophotometers.

The majority of photonic hydrogel sensors have been created by self-assembly. However, most approaches require lengthy synthesis to create Bragg gratings. For example, forming monodisperse, highly-charged polystyrene particles through emulsion polymerization require lengthy dialysis times. The creation of high-quality CCAs with large areas still require hours to days to complete. Furthermore, CCAs suffer from defects since the properties of these highly charged particles cannot be controlled precisely. Other self-assembly approaches including layer-by-layer deposition and spin coating suffer from instability and time-consuming fabrication. For instance, formation of organic-inorganic Bragg stacks is limited due to the instability of the polymer in the presence of acidic inorganic sol, which distorts the morphological integrity of the sublayer.

Inclusion of charged functional groups during self-assembly and polymerization disrupts the lattice spacing in CCAs, block copolymers, and Bragg stacks. Hence, the functionalization of the polymer matrix often needs to be performed post-hydrogel formation. This results in nonuniform distributions of functional moieties throughout the hydrogel matrix. In inverse opals, the diffraction efficiency is relatively higher as compared to the CCAs, but they also suffer from lattice disruption. Furthermore, block copolymers such as PS-b-PAA and PS-b-P2VP are fundamentally limited to pH and unspecific solvent sensing. Additionally, self-assembly approaches lack flexibility in controlling the dimensions of the sensors. For instance, sedimentation and centrifugation do not have precise control over sample thickness. Other approaches involving layer-by-layer deposition is limited to thin films. Although many applications have been demonstrated utilizing self-assembled sensors, few of them utilized the entire visible spectrum to report on the analyte concentrations. Most applications have wavelength shifts smaller than 10 nm, not visible to the eye. In particular, due to high crosslinker concentration, MIPs suffer from small wavelength shifts. Hence, tuning range of Bragg peak shifts requires improvement in polymer synthesis, potentially involving increased porosity and hydrophilicity. Broad wavelength shifts and the entire visible spectrum need to be utilized for practical colorimetric sensing applications.

In contrast to self-assembly, top-down techniques such as holographic patterning offers reproducibility. In fabricating holographic sensors, charged functional groups can be incorporated during polymerization prior to Bragg grating formation. The lattice spacing of

holographic sensors can be easily tuned using different wavelengths of laser light. A challenge associated with holographic sensing is that achieving high diffraction efficiency requires multiple processing steps in silver halide chemistry. While high-energy laser patterning of holographic sensors can be completed in a few steps, this approach suffers from low diffraction efficiency (<10%). Photopolymerization-induced formation of Bragg gratings is a practical approach to create Bragg gratings; however, the migration of short polymer chains during high-intensity recording results in low diffraction efficiency. Nevertheless, holographic patterning offers fabrication flexibility that cannot be achieved with bottom-up approaches.

Hydrogel microlenses provide a simpler fabrication approach as compared to the Bragg grating-based hydrogel sensors. This approach does not require complicated fabrication approaches, and the output of the assay is the changes in the refractive index or the focus of the lens. However, this approach requires significant changes in the refractive index to create a resolvable shift in the spectrophotometer fiber. This approach also falls short as a mobile rapid diagnostic assay since the measurements require an external photodetector. Fiber optic sensors incorporate the hydrogel and a quantitative spectrometry within the same device; and since the hydrogel matrix is in direct contact with the fiber, the readouts are more accurate compared to other sensing platforms. Furthermore, plasmonics is a flexible approach to create photonic hydrogel sensors, but the ability to tune the colors of plasmonic assays and the capability to obtain color changes in the entire visible spectrum is not possible, limiting the use of this assay to yes/no readouts or spectrophotometric analysis.

Existing IVD technologies are primarily based on molecular dyes, electrochemistry, and gold nanoparticle-based lateral-flow assays. These assays cannot colorimetrically display quantitative results, and they cannot be used for repeat analyses. Additionally, the incorporation of many recognition agents using a single platform is challenging for existing assays. This market gap represents an opportunity to develop quantitative photonic hydrogel sensors that can operate in the entire visible spectrum. Photonic hydrogels should offer improvement in sensitivity, selectivity, response time, and user interface to create a competitive advantage. Potential applications may focus on reusable, wearable, and equipment-free colorimetric IVD devices. Another niche area is localized sensing and mapping the concentrations of analytes throughout a smeared sample. The value of photonic hydrogel sensors can only be realized if they offer a strategic advance over existing products, are compatible with existing manufacturing lines, and show efficacy at point-of-care settings.

Author Contributions

A.K.Y. and S.H.Y. designed the review. A.K.Y. wrote the manuscript. L.R.V. contributed to Crystalline Colloidal Array Sensors. M.H. contributed to Refractive Index Modulation-Based Hydrogel Sensors. S.H.Y., L.R.V., I.P., I.N., K.S.K., H.K., S.K.H., S.J.J.K, and A.K. intellectually contributed and edited the manuscript.

Acknowledgements

This work was supported in part by the National Institute of Health (P41EB015903), National Science Foundation (ECCS-1505569, CBET-264356), Department of Defence (FA9550-11-1-0331), the Bio & Medical Technology Development Program (No. 2012M3A9C6049791) and IT Consilience Creative Program (No. NIPA-2014-H0201-14-1001). M.H. was supported by Marie Curie International Outgoing Fellowship (No. 627274). We thank Jeff Blyth, Sanford Asher, and Geoffrey A. Ozin for discussions.

References

Aguirre CI, Reguera E, Stein A. Tunable colors in opals and inverse opal photonic crystals. Adv Funct Mater. 2010;20:2565-78.

Akram MS, Daly R, Vasconcellos FC, Yetisen AK, Hutchings I, Hall EAH. Applications of Paper-Based Diagnostics. In: Castillo-León J, Svendsen WE, editors. Lab-on-a-Chip Devices and Micro-Total Analysis Systems: Springer International Publishing; 2015. p. 161-95.

Alexeev VL, Sharma AC, Goponenko AV, Das S, Lednev IK, Wilcox CS, et al. High ionic strength glucose-sensing photonic crystal. Anal Chem. 2003;75:2316-23.

Anzai J-i, Kobayashi Y, Nakamura N, Nishimura M, Hoshi T. Layer-by-layer construction of multilayer thin films composed of avidin and biotin-labeled poly (amine) s. Langmuir. 1999;15:221-6.

Araki K, Wagner MJ, Wrighton MS. Layer-by-layer growth of electrostatically assembled multilayer porphyrin films. Langmuir. 1996;12:5393-8.

Archer F. On the Use of Collodion in Photography. The Chemist. 1851;2:257-8.

Arsenault A, Fleischhaker F, von Freymann G, Kitaev V, Miguez H, Mihi A, et al. Perfecting imperfection—designer defects in colloidal photonic crystals. Adv Mater. 2006;18:2779-85.

Arunbabu D, Sannigrahi A, Jana T. Photonic crystal hydrogel material for the sensing of toxic mercury ions (Hg 2+) in water. Soft Matter. 2011;7:2592-9.

Asher SA. Crystalline colloidal narrow band radiation filter. 1986.

Asher SA, Alexeev VL, Goponenko AV, Sharma AC, Lednev IK, Wilcox CS, et al. Photonic crystal carbohydrate sensors: low ionic strength sugar sensing. J Am Chem Soc. 2003;125:3322-9.

Asher SA, Holtz J, Liu L, Wu Z. Self-assembly motif for creating submicron periodic materials. Polymerized crystalline colloidal arrays. Journal of the American Chemical Society. 1994;116:4997-8.

Asher SA, Holtz JH. Novel polymerized crystalline colloidal array sensors. 1998.

Asher SA, Peteu SF, Reese CE, Lin M, Finegold D. Polymerized crystalline colloidal array chemical-sensing materials for detection of lead in body fluids. Analytical and bioanalytical chemistry. 2002;373:632-8.

Ayyub OB, Ibrahim MB, Briber RM, Kofinas P. Self-assembled block copolymer photonic crystal for selective fructose detection. Biosens Bioelectron. 2013;46:124-9.

Baca JT, Finegold DN, Asher SA. Progress in developing polymerized crystalline colloidal array sensors for point-of-care detection of myocardial ischemia. Analyst. 2008;133:385-90.

Bachmann C. Outcome and survival of 88 patients with urea cycle disorders: a retrospective evaluation. European journal of pediatrics. 2003;162:410-6.

Banwell EF, Abelardo ES, Adams DJ, Birchall MA, Corrigan A, Donald AM, et al. Rational design and application of responsive α-helical peptide hydrogels. Nat Mater. 2009;8:596-600.

Barry RA, Wiltzius P. Humidity-sensing inverse opal hydrogels. Langmuir. 2006;22:1369-74.

Bates FS, Fredrickson GH. Block copolymer thermodynamics: theory and experiment. Annu Rev Phys Chem. 1990;41:525-57.

Bates FS, Fredrickson GH. Block copolymers—designer soft materials. Phys Today. 2008;52:32-8.

Bhatta D, Christie G, Blyth J, Lowe CR. Development of a holographic sensor for the detection of calcium dipicolinate—A sensitive biomarker for bacterial spores. Sens Actuators, B. 2008;134:356-9.

Bhatta D, Christie G, Madrigal-Gonzalez B, Blyth J, Lowe CR. Holographic sensors for the detection of bacterial spores. Biosens Bioelectron. 2007;23:520-7.
Blanquart-Evrard L-D. Procédés employés pour obtenir les épreuves de photographie sur papier: C. Chevalier; 1847.
Blyth J, Millington RB, Mayes AG, Frears ER, Lowe CR. Holographic sensor for water in solvents. Anal Chem. 1996;68:1089-94.
Blyth J, Millington RB, Mayes AG, Lowe CR. A diffusion method for making silver bromide based holographic recording material. Imaging Sci J. 1999;47:87-92.
Bockstaller M, Kolb R, Thomas EL. Metallodielectric photonic crystals based on diblock copolymers. Adv Mater. 2001;13:1783-6.
Bockstaller MR, Mickiewicz RA, Thomas EL. Block copolymer nanocomposites: perspectives for tailored functional materials. Adv Mater. 2005;17:1331-49.
Bonanno LM, DeLouise LA. Whole blood optical biosensor. Biosens Bioelectron. 2007;23:444-8.
Bonanno LM, DeLouise LA. Integration of a Chemical-Responsive Hydrogel into a Porous Silicon Photonic Sensor for Visual Colorimetric Readout. Adv Funct Mater. 2010;20:573-8.
Bonanno LM, Kwong TC, DeLouise LA. Label-free porous silicon immunosensor for broad detection of opiates in a blind clinical study and results comparison to commercial analytical chemistry techniques. Anal Chem. 2010;82:9711-8.
Bonifacio LD, Lotsch BV, Puzzo DP, Scotognella F, Ozin GA. Stacking the Nanochemistry Deck: Structural and Compositional Diversity in One-Dimensional Photonic Crystals. Adv Mater. 2009;21:1641-6.
Boulmedais F, Ball V, Schwinte P, Frisch B, Schaaf P, Voegel J-C. Buildup of exponentially growing multilayer polypeptide films with internal secondary structure. Langmuir. 2003;19:440-5.
Brust M, Walker M, Bethell D, Schiffrin DJ, Whyman R. Synthesis of thiol-derivatised gold nanoparticles in a two-phase liquid–liquid system. J Chem Soc, Chem Commun. 1994:801-2.
Brynda E, Houska M. Multiple alternating molecular layers of albumin and heparin on solid surfaces. J Colloid Interface Sci. 1996;183:18-25.
Bucknall DG, Anderson HL. Polymers get organized. Science. 2003;302:1904-5.
Buenger D, Topuz F, Groll J. Hydrogels in sensing applications. Prog Polym Sci. 2012;37:1678-719.
Burgess IB, Loncar M, Aizenberg J. Structural colour in colourimetric sensors and indicators. J Mater Chem C. 2013;1:6075-86.
Butt H, Yetisen AK, Ahmed R, Yun SH, Dai Q. Carbon nanotube biconvex microcavities. Appl Phys Lett. 2015;106:121108.
Cai Z, Liu YJ, Lu X, Teng J. In situ “doping” inverse silica opals with size-controllable gold nanoparticles for refractive index sensing. J Phys Chem C. 2013;117:9440-5.
Cai Z, Smith NL, Zhang J-T, Asher SA. Two-Dimensional Photonic Crystal Chemical and Biomolecular Sensors. Anal Chem. 2015;87:5013-25.
Cai Z, Zhang J-T, Xue F, Hong Z, Punihaole D, Asher SA. 2D photonic crystal protein hydrogel coulometer for sensing serum albumin ligand binding. Anal Chem. 2014;86:4840-7.
Carlson RJ, Asher SA. Characterization of optical diffraction and crystal structure in monodisperse polystyrene colloids. Applied spectroscopy. 1984;38:297-304.
Cate DM, Adkins JA, Mettakoonpitak J, Henry CS. Recent Developments in Paper-Based Microfluidic Devices. Anal Chem. 2015;87:19-41.

Cennamo N, D'Agostino G, Galatus R, Bibbo L, Pesavento M, Zeni L. Sensors based on surface plasmon resonance in a plastic optical fiber for the detection of trinitrotoluene. Sens Actuators, B. 2013;188:221-6.
Chen C, Zhu Y, Bao H, Shen J, Jiang H, Peng L, et al. Ethanol-assisted multi-sensitive poly (vinyl alcohol) photonic crystal sensor. Chem Commun (Cambridge, U K). 2011;47:5530-2.
Chiappelli MC, Hayward RC. Photonic Multilayer Sensors from Photo-Crosslinkable Polymer Films. Adv Mater. 2012;24:6100-4.
Chin CD, Linder V, Sia SK. Commercialization of microfluidic point-of-care diagnostic devices. Lab Chip. 2012;12:2118-34.
Chiu JJ, Kim BJ, Kramer EJ, Pine DJ. Control of nanoparticle location in block copolymers. J Am Chem Soc. 2005;127:5036-7.
Chiu JJ, Kim BJ, Yi G-R, Bang J, Kramer EJ, Pine DJ. Distribution of nanoparticles in lamellar domains of block copolymers. Macromolecules. 2007;40:3361-5.
Choi CJ, Cunningham BT. A 96-well microplate incorporating a replica molded microfluidic network integrated with photonic crystal biosensors for high throughput kinetic biomolecular interaction analysis. Lab Chip. 2007;7:550-6.
Choi M, Choi JW, Kim S, Nizamoglu S, Hahn SK, Yun SH. Light-guiding hydrogels for cell-based sensing and optogenetic synthesis in vivo. Nature Photon. 2013;7:987-94.
Cooper TM, Campbell AL, Crane RL. Formation of polypeptide-dye multilayers by electrostatic self-assembly technique. Langmuir. 1995;11:2713-8.
Couturier JP, Sütterlin M, Laschewsky A, Hettrich C, Wischerhoff E. Responsive Inverse Opal Hydrogels for the Sensing of Macromolecules. Angew Chem, Int Ed. 2015;54:6641-4.
Cui J, Zhu W, Gao N, Li J, Yang H, Jiang Y, et al. Inverse Opal Spheres Based on Polyionic Liquids as Functional Microspheres with Tunable Optical Properties and Molecular Recognition Capabilities. Angew Chem, Int Ed. 2014;53:3844-8.
Danaei G, Finucane MM, Lu Y, Singh GM, Cowan MJ, Paciorek CJ, et al. National, regional, and global trends in fasting plasma glucose and diabetes prevalence since 1980: systematic analysis of health examination surveys and epidemiological studies with 370 country-years and 2· 7 million participants. Lancet. 2011;378:31-40.
Decher G. Fuzzy nanoassemblies: toward layered polymeric multicomposites. Science. 1997;277:1232-7.
Decher G, Hong J. Buildup of ultrathin multilayer films by a self-assembly process: II. Consecutive adsorption of anionic and cationic bipolar amphiphiles and polyelectrolytes on charged surfaces. Ber Bunsenges Phys Chem. 1991;95:1430-4.
Decher G, Hong J, Schmitt J. Buildup of ultrathin multilayer films by a self-assembly process: III. Consecutively alternating adsorption of anionic and cationic polyelectrolytes on charged surfaces. Thin solid films. 1992;210:831-5.
DeLouise LA, Fauchet PM, Miller BL, Pentland AA. Hydrogel-Supported Optical-Microcavity Sensors. Adv Mater. 2005;17:2199-203.
Deng S, Yetisen AK, Jiang K, Butt H. Computational modelling of a graphene Fresnel lens on different substrates. RSC Adv. 2014;4:30050-8.
Denisyuk YN. On the reflection of optical properties of an object in a wave field of light scattered by it. Dokl Akad Nauk SSSR. 1962;144:1275.
DiabetesAtlas. 6 edn. International Diabetes Federation. 2013.

Diao YY, Liu XY, Toh GW, Shi L, Zi J. Multiple Structural Coloring of Silk-Fibroin Photonic Crystals and Humidity-Responsive Color Sensing. Advanced Functional Materials. 2013;23:5373-80.
Domschke A, March WF, Kabilan S, Lowe C. Initial clinical testing of a holographic non-invasive contact lens glucose sensor. Diabetes Technol Ther. 2006;8:89-93.
Dong L, Agarwal AK, Beebe DJ, Jiang H. Adaptive liquid microlenses activated by stimuli-responsive hydrogels. Nature. 2006;442:551-4.
Dziri L, Boussaad S, Tao N, Leblanc RM. Acetylcholinesterase complexation with acetylthiocholine or organophosphate at the air/aqueous interface: AFM and UV-Vis studies. Langmuir. 1998;14:4853-9.
Edrington AC, Urbas AM, DeRege P, Chen CX, Swager TM, Hadjichristidis N, et al. Polymer-based photonic crystals. Adv Mater. 2001;13:421-5.
Egen M, Voss R, Griesebock B, Zentel R, Romanov S, Torres CS. Heterostructures of Polymer Photonic Crystal Films. Chem Mater. 2003;15:3786-92.
Ehrbar M, Schoenmakers R, Christen EH, Fussenegger M, Weber W. Drug-sensing hydrogels for the inducible release of biopharmaceuticals. Nat Mater. 2008;7:800-4.
Ehrick JD, Deo SK, Browning TW, Bachas LG, Madou MJ, Daunert S. Genetically engineered protein in hydrogels tailors stimuli-responsive characteristics. Nat Mater. 2005;4:298-302.
Ehrick JD, Stokes S, Bachas-Daunert S, Moschou EA, Deo SK, Bachas LG, et al. Chemically Tunable Lensing of Stimuli-Responsive Hydrogel Microdomes. Adv Mater. 2007;19:4024-7.
Farandos NM, Yetisen AK, Monteiro MJ, Lowe CR, Yun SH. Contact Lens Sensors in Ocular Diagnostics. Adv Healthc Mater. 2015;4:792-810.
Ferrand P, Egen M, Zentel R, Seekamp J, Romanov S, Torres CS. Structuring of self-assembled three-dimensional photonic crystals by direct electron-beam lithography. Appl Phys Lett. 2003;83:5289-91.
Fink Y, Urbas AM, Bawendi MG, Joannopoulos JD, Thomas EL. Block copolymers as photonic bandgap materials. J Lightwave Technol. 1999;17:1963-9.
Fleischhaker F, Arsenault AC, Kitaev V, Peiris FC, von Freymann G, Manners I, et al. Photochemically and thermally tunable planar defects in colloidal photonic crystals. J Am Chem Soc. 2005a;127:9318-9.
Fleischhaker F, Arsenault AC, Peiris FC, Kitaev V, Manners I, Zentel R, et al. DNA designer defects in photonic crystals: Optically monitored biochemistry. Adv Mater. 2006;18:2387-91.
Fleischhaker F, Arsenault AC, Wang Z, Kitaev V, Peiris FC, von Freymann G, et al. Redox-Tunable Defects in Colloidal Photonic Crystals. Adv Mater. 2005b;17:2455-8.
Folke M, Cernerud L, Ekström M, Hök B. Critical review of non-invasive respiratory monitoring in medical care. Med Biol Eng Comput. 2003;41:377-83.
Fredrickson GH, Bates FS. Dynamics of block copolymers: theory and experiment. Annu Rev Mater Sci. 1996;26:501-50.
Fuchs Y, Kunath S, Soppera O, Haupt K, Mayes AG. Molecularly Imprinted Silver-Halide Reflection Holograms for Label-Free Opto-Chemical Sensing. Adv Funct Mater. 2014;24:688-94.
Fuchs Y, Soppera O, Mayes AG, Haupt K. Holographic molecularly imprinted polymers for label-free chemical sensing. Adv Mater. 2013;25:566-70.
Fudouzi H. Tunable structural color in organisms and photonic materials for design of bioinspired materials. Sci Tech Adv Mater. 2011;12:064704.

Furumi S, Fudouzi H, Sawada T. Self-organized colloidal crystals for photonics and laser applications. Laser Photonics Rev. 2010;4:205-20.
Gabor D. A new microscopic principle. Nature. 1948;161:777-8.
Gabor D. Microscopy by reconstructed wave-fronts. Proc R Soc A. 1949;197:454-87.
Ge J, Yin Y. Responsive photonic crystals. Angew Chem, Int Ed. 2011;50:1492-522.
Gerlach G, Arndt K-F. Hydrogel sensors and actuators: engineering and technology. Heidelberg: Springer Science & Business Media; 2009.
Gonzalez BM, Christie G, Davidson CAB, Blyth J, Lowe CR. Divalent metal ion-sensitive holographic sensors. Anal Chim Acta. 2005;528:219-28.
GrandViewResearch. In-Vitro Diagnostics (IVD) Market Analysis and Segment Forecasts To 2020. 2014.
Griffete N, Frederich H, Maître A, Ravaine S, Chehimi MM, Mangeney C. Inverse Opals of Molecularly Imprinted Hydrogels for the Detection of Bisphenol A and pH Sensing. Langmuir. 2012;28:1005-12.
Guo C, Zhou C, Sai N, Ning B, Liu M, Chen H, et al. Detection of bisphenol A using an opal photonic crystal sensor. Sens Actuators, B. 2012;166:17-23.
Haacke G, Panzer HP, Magliocco LG, Asher SA. Narrow band radiation filter films. 1993.
Hadziioannou G, Skoulios A. Molecular weight dependence of lamellar structure in styrene isoprene two-and three-block copolymers. Macromolecules. 1982;15:258-62.
Haslam RH. Lead poisoning. Paediatrics & child health. 2003;8:509.
Hazell AS, Butterworth RF. Hepatic encephalopathy: An update of pathophysiologic mechanisms. Experimental Biology and Medicine. 1999;222:99-112.
He J-A, Valluzzi R, Yang K, Dolukhanyan T, Sung C, Kumar J, et al. Electrostatic multilayer deposition of a gold-dendrimer nanocomposite. Chem Mater. 1999;11:3268-74.
Heskins M, Guillet JE. Solution properties of poly (N-isopropylacrylamide). Journal of Macromolecular Science—Chemistry. 1968;2:1441-55.
Hinterholzinger FM, Ranft A, Feckl JM, Ruhle B, Bein T, Lotsch BV. One-dimensional metal-organic framework photonic crystals used as platforms for vapor sorption. J Mater Chem. 2012;22:10356-62.
Hisamitsu I, Kataoka K, Okano T, Sakurai Y. Glucose-responsive gel from phenylborate polymer and poly (vinyl alcohol): prompt response at physiological pH through the interaction of borate with amino group in the gel. Pharmaceutical research. 1997;14:289-93.
Holtz JH, Asher SA. Polymerized colloidal crystal hydrogel films as intelligent chemical sensing materials. Nature. 1997;389:829-32.
Holtz JH, Holtz JS, Munro CH, Asher SA. Intelligent polymerized crystalline colloidal arrays: novel chemical sensor materials. Analytical Chemistry. 1998;70:780-91.
Hong J, Lowack K, Schmitt J, Decher G. Layer-by-layer deposited multilayer assemblies of polyelectrolytes and proteins: from ultrathin films to protein arrays. In: Laggner P, Glatter O, editors. Trends in Colloid and Interface Science VII: Springer; 1993. p. 98-102.
Hong W, Chen Y, Feng X, Yan Y, Hu X, Zhao B, et al. Full-color CO2 gas sensing by an inverse opal photonic hydrogel. Chem Commun (Cambridge, U K). 2013;49:8229-31.
Hong W, Li H, Hu X, Zhao B, Zhang F, Zhang D. Independent multifunctional detection by wettability controlled inverse opal hydrogels. Chem Commun (Cambridge, U K). 2012;48:4609-11.
Hooke R. Micrographia. London: J. Martyn and J. Allestry; 1665.

Horgan AM, Marshall AJ, Kew SJ, Dean KES, Creasey CD, Kabilan S. Crosslinking of phenylboronic acid receptors as a means of glucose selective holographic detection. Biosens Bioelectron. 2006;21:1838-45.
Huang H, Serpe MJ. Poly (N-isopropylacrylamide) microgel-based etalons for determining the concentration of ethanol in gasoline. J Appl Polym Sci. 2015;132.
Hurtado JL, Lowe CR. Ammonia-sensitive photonic structures fabricated in nafion membranes by laser ablation. ACS Appl Mater Interfaces. 2014;6:8903-8.
Imran AB, Seki T, Takeoka Y. Recent advances in hydrogels in terms of fast stimuli responsiveness and superior mechanical performance. Polym J. 2010;42:839-51.
Ingersoll D, Kulesza PJ, Faulkner LR. Polyoxometallate-Based Layered Composite Films on Electrodes Preparation Through Alternate Immersions in Modification Solutions. J Electrochem Soc. 1994;141:140-7.
Islam MR, Serpe MJ. A novel label-free colorimetric assay for DNA concentration in solution. Anal Chim Acta. 2014;843:83-8.
Jiang C, Ko H, Tsukruk VV. Strain-Sensitive Raman Modes of Carbon Nanotubes in Deflecting Freely Suspended Nanomembranes. Adv Mater. 2005;17:2127-31.
Jiang H, Markowski J, Sabarinathan J. Near-infrared optical response of thin film pH-sensitive hydrogel coated on a gold nanocrescent array. Opt Express. 2009;17:21802-7.
Jiang H, Zhu Y, Chen C, Shen J, Bao H, Peng L, et al. Photonic crystal pH and metal cation sensors based on poly (vinyl alcohol) hydrogel. New J Chem. 2012;36:1051-6.
Jin L, Zhao Y, Liu X, Wang Y, Ye B, Xie Z, et al. Dual signal glucose reporter based on inverse opal conducting hydrogel films. Soft Matter. 2012;8:4911-7.
Joannopoulos JD, Johnson SG, Winn JN, Meade RD. Photonic crystals: molding the flow of light. 2 ed. United States: Princeton University Press; 2011.
Kabilan S, Blyth J, Lee MC, Marshall AJ, Hussain A, Yang XP, et al. Glucose-sensitive holographic sensors. J Mol Recognit. 2004;17:162-6.
Kabilan S, Marshall AJ, Sartain FK, Lee MC, Hussain A, Yang XP, et al. Holographic glucose sensors. Biosens Bioelectron. 2005;20:1602-10.
Kado S, Otani H, Nakahara Y, Kimura K. Highly selective recognition of acetate and bicarbonate by thiourea-functionalised inverse opal hydrogel in aqueous solution. Chem Commun (Cambridge, U K). 2013;49:886-8.
KaloramaInformation. The Market and Potential for Molecular Point of Care Diagnostics. 2014.
Kang Y, Walish JJ, Gorishnyy T, Thomas EL. Broad-wavelength-range chemically tunable block-copolymer photonic gels. Nat Mater. 2007;6:957-60.
Keller SW, Kim H-N, Mallouk TE. Layer-by-Layer Assembly of intercalation compounds and heterostructures on surfaces: Toward molecular" beaker" epitaxy. J Am Chem Soc. 1994;116:8817-8.
Kim H-C, Park S-M, Hinsberg WD. Block copolymer based nanostructures: materials, processes, and applications to electronics. Chem Rev. 2010;110:146-77.
Kim J, Nayak S, Lyon LA. Bioresponsive hydrogel microlenses. J Am Chem Soc. 2005a;127:9588-92.
Kim J, Serpe MJ, Lyon LA. Hydrogel microparticles as dynamically tunable microlenses. J Am Chem Soc. 2004;126:9512-3.
Kim J, Serpe MJ, Lyon LA. Photoswitchable Microlens Arrays. Angew Chem, Int Ed. 2005b;44:1333-6.

Kim J, Singh N, Lyon LA. Label-Free Biosensing with Hydrogel Microlenses. Angew Chem, Int Ed. 2006;45:1446-9.
Kim J, Singh N, Lyon LA. Displacement-Induced Switching Rates of Bioresponsive Hydrogel Microlenses. Chem Mater. 2007a;19:2527-32.
Kim J, Singh N, Lyon LA. Influence of ancillary binding and nonspecific adsorption on bioresponsive hydrogel microlenses. Biomacromolecules. 2007b;8:1157-61.
Kim O-H, Cho Y-H, Kang SH, Park H-Y, Kim M, Lim JW, et al. Ordered macroporous platinum electrode and enhanced mass transfer in fuel cells using inverse opal structure. Nat Commun. 2013;4.
Kim S-H, Park J-G, Choi TM, Manoharan VN, Weitz DA. Osmotic-pressure-controlled concentration of colloidal particles in thin-shelled capsules. Nat Commun. 2014;5.
Kimble KW, Walker JP, Finegold DN, Asher SA. Progress toward the development of a point-of-care photonic crystal ammonia sensor. Analytical and bioanalytical chemistry. 2006;385:678-85.
Kleinfeld ER, Ferguson GS. Stepwise formation of multilayered nanostructural films from macromolecular precursors. Science. 1994;265:370-3.
Klinger D, Robb MJ, Spruell JM, Lynd NA, Hawker CJ, Connal LA. Supramolecular guests in solvent driven block copolymer assembly: from internally structured nanoparticles to micelles. Polym Chem. 2013;4:5038-42.
Kloxin AM, Kasko AM, Salinas CN, Anseth KS. Photodegradable hydrogels for dynamic tuning of physical and chemical properties. Science. 2009;324:59-63.
Komatsu H, Miyachi M, Fujii E, Citterio D, Yamada K, Sato Y, et al. SPR sensor signal amplification based on dye-doped polymer particles. Sci Technol Adv Mater. 2006;7:150-5.
Kong W, Zhang X, Gao ML, Zhou H, Li W, Shen JC. A new kind of immobilized enzyme multilayer based on cationic and anionic interaction. Macromol Rapid Commun. 1994;15:405-9.
Kong X-T, Butt H, Yetisen AK, Kangwanwatana C, Montelongo Y, Deng S, et al. Enhanced reflection from inverse tapered nanocone arrays. Appl Phys Lett. 2014;105:053108.
Kong X-T, Khan AA, Kidambi PR, Deng S, Yetisen AK, Dlubak B, et al. Graphene-Based Ultrathin Flat Lenses. ACS Photonics. 2015;2:200-7.
Kotov NA. Layer-by-layer self-assembly: The contribution of hydrophobic interactions. Nanostruct Mater. 1999;12:789-96.
Kotov NA, Dekany I, Fendler JH. Layer-by-Layer Self-Assembly of Polyelectrolyte-Semiconductor Nanoparticle Composite Films. J Phys Chem. 1995;99:13065-9.
Kraiskii AV, Postnikov VA, Sultanov TT, Khamidulin AV. Holographic sensors for diagnostics of solution components. IEEE J Quantum Electron. 2010;40:178-82.
Kratz A. Laboratory reference values (vol 351, pg 1548, 2004). New Engl J Med. 2004;351:2461-.
Ku KH, Shin JM, Kim MP, Lee C-H, Seo M-K, Yi G-R, et al. Size-Controlled Nanoparticle-Guided Assembly of Block Copolymers for Convex Lens-Shaped Particles. J Am Chem Soc. 2014;136:9982-9.
Kuriu Y, Kawamura A, Uragami T, Miyata T. Formation of Thin Molecularly Imprinted Hydrogel Layers with Lectin Recognition Sites on SPR Sensor Chips by Atom Transfer Radical Polymerization. Chem Lett. 2014;43:825-7.
Lavine BK, Oxenford L, Kim M, Kaval N, Benjamin M, Seitz W. Novel turbidimetric method to study polymer swelling. Microchem J. 2012;103:97-104.

Lee K, Asher SA. Photonic crystal chemical sensors: pH and ionic strength. Journal of the American Chemical Society. 2000;122:9534-7.
Lee MC, Kabilan S, Hussain A, Yang X, Blyth J, Lowe CR. Glucose-sensitive holographic sensors for monitoring bacterial growth. Anal Chem. 2004a;76:5748-55.
Lee W, Pruzinsky SA, Braun PV. Multi-photon polymerization of waveguide structures within three-dimensional photonic crystals. Adv Mater. 2002;14:271.
Lee Y-J, Pruzinsky SA, Braun PV. Glucose-sensitive inverse opal hydrogels: analysis of optical diffraction response. Langmuir. 2004b;20:3096-106.
Lee YJ, Braun PV. Tunable inverse opal hydrogel pH sensors. Adv Mater. 2003;15:563-6.
Leite E, Babeva T, Ng EP, Toal V, Mintova S, Naydenova I. Optical Properties of Photopolymer Layers Doped with Aluminophosphate Nanocrystals. J Phys Chem C. 2010a;114:16767-75.
Leite E, Naydenova I, Mintova S, Leclercq L, Toal V. Photopolymerizable nanocomposites for holographic recording and sensor application. Appl Opt. 2010b;49:3652-60.
Leith EN, Upatnieks J. Reconstructed Wavefronts and Communication Theory. J Opt Soc Am. 1962;52:1123-8.
Lelong A, Hégaret H, Soudant P, Bates SS. Pseudo-nitzschia (Bacillariophyceae) species, domoic acid and amnesic shellfish poisoning: revisiting previous paradigms. Phycologia. 2012;51:168-216.
Lendlein A, Jiang H, Jünger O, Langer R. Light-induced shape-memory polymers. Nature. 2005;434:879-82.
Li C, Lotsch BV. Stimuli-responsive 2D polyelectrolyte photonic crystals for optically encoded pH sensing. Chem Commun (Cambridge, U K). 2012;48:6169-71.
Li S, Yang M, Zhou W, Johnston TG, Wang R, Zhu J. Dextran Hydrogel Coated Surface Plasmon Resonance Imaging (SPRi) Sensor for Sensitive and Label-free Detection of Small Molecule Drugs. Appl Surf Sci. 2015a.
Li X, Gao Y, Serpe MJ. Reductant-responsive poly (N-isopropylacrylamide) microgels and microgel-based optical materials. Can J Chem. 2015b;93:1-5.
Li X, Peng L, Cui J, Li W, Lin C, Xu D, et al. Reactive Photonic Film for Label-Free and Selective Sensing of Cyanide. Small. 2012;8:612-8.
Lim HS, Lee J-H, Walish JJ, Thomas EL. Dynamic swelling of tunable full-color block copolymer photonic gels via counterion exchange. ACS Nano. 2012;6:8933-9.
Lin F-Y, Yu L-P. Thiourea functionalized hydrogel photonic crystal sensor for Cd 2+ detection. Anal Methods. 2012;4:2838-45.
Lippmann G. Sur la Theorie de la Photographie des Couleurs Simples et Composees par la Methode Interferentielle. J Phys. 1894;3:97–107.
Liu C, Gao G, Zhang Y, Wang L, Wang J, Song Y. The Naked-Eye Detection of NH3–HCl by Polyaniline-Infiltrated TiO2 Inverse Opal Photonic Crystals. Macromol Rapid Commun. 2012;33:380-5.
Liu S, Volkmer D, Kurth DG. Functional polyoxometalate thin films via electrostatic layer-by-layer self-assembly. J Cluster Sci. 2003;14:405-19.
Lockwood AH. Blood ammonia levels and hepatic encephalopathy. Metabolic brain disease. 2004;19:345-9.
Loh XJ, Scherman OA. Polymeric and Self Assembled Hydrogels: From Fundamental Understanding to Applications. Cambridge, UK: Royal Society of Chemistry; 2012.
Loiseaux B, Huignard JP, Dubois JC, Eranian A. Process for producing diffracting phase structures. 1984.

Lojou É, Bianco P. Buildup of polyelectrolyte-protein multilayer assemblies on gold electrodes. Role of the hydrophobic effect. Langmuir. 2004;20:748-55.
Lotierzo M, Henry OYF, Piletsky S, Tothill I, Cullen D, Kania M, et al. Surface plasmon resonance sensor for domoic acid based on grafted imprinted polymer. Biosens Bioelectron. 2004;20:145-52.
Lotsch BV, Knobbe CB, Ozin GA. A Step Towards Optically Encoded Silver Release in 1D Photonic Crystals. Small. 2009;5:1498-503.
Lowe CR, Millington RB, Blyth J, Mayes AG. Hologram used as a sensor, WO Patent Application 1995026499 A1. 1995.
Lvov Y, Ariga K, Ichinose I, Kunitake T. Assembly of multicomponent protein films by means of electrostatic layer-by-layer adsorption. J Am Chem Soc. 1995;117:6117-23.
Lvov Y, Ariga K, Kunitake T. Layer-by-Layer Assembly of Alternate Protein/Polyion Ultrathin Films. Chem Lett. 1994:2323-6.
Lvov Y, Decher G, Sukhorukov G. Assembly of thin films by means of successive deposition of alternate layers of DNA and poly (allylamine). Macromolecules. 1993;26:5396-9.
Lvov Y, ONDA M, ARIGA K, KUNITAKE T. Ultrathin films of charged polysaccharides assembled alternately with linear polyions. J Biomater Sci, Polym Ed. 1998;9:345-55.
Lynd NA, Meuler AJ, Hillmyer MA. Polydispersity and block copolymer self-assembly. Prog Polym Sci. 2008;33:875-93.
Lyon LA, Debord JD, Debord SB, Jones CD, McGrath JG, Serpe MJ. Microgel Colloidal Crystals. J Phys Chem B. 2004;108:19099-108.
Ma C, Jiang Y, Yang X, Wang C, Li H, Dong F, et al. Centrifugation-Induced Water-Tunable Photonic Colloidal Crystals with Narrow Diffraction Bandwidth and Highly Sensitive Detection of SCN–. ACS Appl Mater Interfaces. 2013;5:1990-6.
MacConaghy KI, Chadly DM, Stoykovich MP, Kaar JL. Optically Diffracting Hydrogels for Screening Kinase Activity in Vitro and in Cell Lysate: Impact of Material and Solution Properties. Anal Chem. 2015;87:3467-75.
Mack NH, Wackerly JW, Malyarchuk V, Rogers JA, Moore JS, Nuzzo RG. Optical Transduction of Chemical Forces. Nano Lett. 2007;7:733-7.
Maddox RL. An Experiment with Gelatino-Bromide. Br J of Photography 1871;18:422-3
Maiman TH. Stimulated Optical Radiation in Ruby. Nature. 1960;187:493-4.
Mamedov AA, Kotov NA, Prato M, Guldi DM, Wicksted JP, Hirsch A. Molecular design of strong single-wall carbon nanotube/polyelectrolyte multilayer composites. Nat Mater. 2002;1:190-4.
Manikas A, Aliberti A, Causa F, Battista E, Netti P. Thermoresponsive PNIPAAm hydrogel scaffolds with encapsulated AuNPs show high analyte-trapping ability and tailored plasmonic properties for high sensing efficiency. J Mater Chem B. 2014;3:53-8.
Mansfield E, O'Leary TJ, Gutman SI. Food and Drug Administration regulation of in vitro diagnostic devices. J Mol Diagn. 2005;7:2-7.
Markets&Markets. In Vitro Diagnostic (IVD) Market [Instruments, Reagents & Data Management Systems] [Technique (Immunoassay, Clinical Chemistry, Molecular Diagnostics, Haematology) & Applications (Diabetes, Infectious Diseases, Cancer & Cardiology)] Systems, End Users] – Forecast To 2017 2013.
Marshall AJ, Blyth J, Davidson CA, Lowe CR. pH-sensitive holographic sensors. Anal Chem. 2003;75:4423-31.

Marshall AJ, Young DS, Blyth J, Kabilan S, Lowe CR. Metabolite-sensitive holographic biosensors. Anal Chem. 2004a;76:1518-23.
Marshall AJ, Young DS, Kabilan S, Hussain A, Blyth J, Lowe CR. Holographic sensors for the determination of ionic strength. Anal Chim Acta. 2004b;527:13-20.
Martinez-Hurtado JL, Akram MS, Yetisen AK. Iridescence in Meat Caused by Surface Gratings. Foods. 2013;2:499-506.
Martinez-Hurtado JL, Davidson CA, Blyth J, Lowe CR. Holographic detection of hydrocarbon gases and other volatile organic compounds. Langmuir. 2010;26:15694-9.
Martinez-Hurtado JL, Davidson CAB, Lowe CR. Monitoring organic volatiles and flammable gases with a holographic sensor. In: Vo-Dinh T, Lieberman RA, Gauglitz G, editors. Proc Spie. Orlando, Florida: Proc. SPIE; 2011. p. 80240Y-1.
Martinez AW, Phillips ST, Whitesides GM. Three-dimensional microfluidic devices fabricated in layered paper and tape. Proceedings of the National Academy of Sciences of the United States of America. 2008;105:19606-11.
Massé P, Reculusa S, Clays K, Ravaine S. Tailoring planar defect in three-dimensional colloidal crystals. Chem Phys Lett. 2006;422:251-5.
Matsen MW, Bates F. Origins of complex self-assembly in block copolymers. Macromolecules. 1996;29:7641-4.
Mayer KM, Hafner JH. Localized surface plasmon resonance sensors. Chem Rev. 2011;111:3828-57.
Mayes AG, Blyth J, Kyröläinen-Reay M, Millington RB, Lowe CR. A Holographic Alcohol Sensor. Anal Chem. 1999;71:3390-6.
Mayes AG, Blyth J, Millington RB, Lowe CR. Metal ion-sensitive holographic sensors. Anal Chem. 2002;74:3649-57.
Mesch M, Zhang C, Braun PV, Giessen H. Functionalized Hydrogel on Plasmonic Nanoantennas for Noninvasive Glucose Sensing. ACS Photonics. 2015;2:475-80.
Mikulchyk T, Martin S, Naydenova I. Humidity and temperature effect on properties of transmission gratings recorded in PVA/AA-based photopolymer layers. J Opt. 2013;15:105301.
Mikulchyk T, Martin S, Naydenova I. Investigation of the sensitivity to humidity of an acrylamide-based photopolymer containing N-phenylglycine as a photoinitiator. Opt Mater. 2014;37:810-5.
Millington RB, Mayes AG, Blyth J, Lowe CR. A hologram biosensor for proteases. Sens Actuators, B. 1996;33:55-9.
Mishra SK, Gupta BD. Surface plasmon resonance based fiber optic pH sensor utilizing Ag/ITO/Al/hydrogel layers. Analyst. 2013;138:2640-6.
Mishra SK, Gupta BD. Surface plasmon resonance based fiber optic sensor for the detection of CrO 4 2− using Ag/ITO/hydrogel layers. Anal Methods. 2014;6:5191-7.
Miyata T. Preparation of smart soft materials using molecular complexes. Polym J. 2010;42:277-89.
Morokoshi S, Ohhori K, Mizukami K, Kitano H. Sensing Capabilities of Colloidal Gold Modified with a Self-Assembled Monolayer of a Glucose-Carrying Polymer Chain on a Glass Substrate†. Langmuir. 2004;20:8897-902.
Müller M. Orientation of α-helical poly (L-lysine) in consecutively adsorbed polyelectrolyte multilayers on texturized silicon substrates. Biomacromolecules. 2001;2:262-9.

Nakayama D, Takeoka Y, Watanabe M, Kataoka K. Simple and precise preparation of a porous gel for a colorimetric glucose sensor by a templating technique. Angew Chem. 2003;115:4329-32.
Naydenova I, Jallapuram R, Martin S, Toal V. Holographic Humidity Sensors. In: Okada CT, editor. Humidity Sensors: Types, Nanomaterials and Environmental Monitoring. Hauppauge: Nova Science Publishers; 2011. p. 117-42.
Naydenova I, Jallapuram R, Toal V, Martin S. A visual indication of environmental humidity using a color changing hologram recorded in a self-developing photopolymer. Appl Phys Lett. 2008;92:031109.
Naydenova I, Jallapuram R, Toal V, Martin S. Characterisation of the humidity and temperature responses of a reflection hologram recorded in acrylamide-based photopolymer. Sens Actuators, B. 2009;139:35-8.
Newton I. Opticks: Or, A Treatise of the Reflections, Refractions, Inflections and Colours of Light. London: Sam. Smith & Benj. Walford; 1704.
Nogueira GM, Banerjee D, Cohen RE, Rubner MF. Spray-Layer-by-Layer Assembly Can More Rapidly Produce Optical-Quality Multistack Heterostructures. Langmuir. 2011;27:7860-7.
Nuopponen M, Tenhu H. Gold Nanoparticles Protected with pH and Temperature-Sensitive Diblock Copolymers. Langmuir. 2007;23:5352-7.
Ock K, Jang G, Roh Y, Kim S, Kim J, Koh K. Optical detection of Cu2+ ion using a SQ-dye containing polymeric thin-film on Au surface. Microchem J. 2001;70:301-5.
Oh J-W, Chung W-J, Heo K, Jin H-E, Lee BY, Wang E, et al. Biomimetic virus-based colourimetric sensors. Nat Commun. 2014;5.
Okumura A, Sato Y, Kyo M, Kawaguchi H. Point mutation detection with the sandwich method employing hydrogel nanospheres by the surface plasmon resonance imaging technique. Anal Biochem. 2005;339:328-37.
Ouyang L, Zhu L, Jiang J, Xie W, Tang H. Three-dimensional plasmonic hydrogel architecture: facile synthesis and its macroscale effective space. RSC Adv. 2015;5:2231-8.
Palacios-Lidón E, Galisteo-López JF, Juárez BH, López C. Engineered planar defects embedded in opals. Adv Mater. 2004;16:341-5.
Palmer JR, Wise LA, Hatch EE, Troisi R, Titus-Ernstoff L, Strohsnitter W, et al. Prenatal diethylstilbestrol exposure and risk of breast cancer. Cancer Epidemiol, Biomarkers Prev. 2006;15:1509-14.
Pan Z, Ma J, Yan J, Zhou M, Gao J. Response of inverse-opal hydrogels to alcohols. J Mater Chem. 2012;22:2018-25.
Park R. IVD Market Continues to Be Steady and Solid, Medical Design Technology Magazine. 2014.
Parmar A. Global In Vitro Diagnostics Market to Grow To $69.1 billion by 2017, Medical Device and Diagnostic Industry Magazine. 2013.
Pike J, Godbert S, Johnson S. Comparison of volunteers' experience of using, and accuracy of reading, different types of home pregnancy test formats. Expert Opin Med Diagn. 2013;7:435-41.
Pozas R, Mihi A, Ocaña M, Míguez H. Building Nanocrystalline Planar Defects within Self-Assembled Photonic Crystals by Spin-Coating. Adv Mater. 2006;18:1183-7.
Price CP, Kricka LJ. Improving healthcare accessibility through point-of-care technologies. Clin Chem. 2007;53:1665-75.

Pruzinsky SA, Braun PV. Fabrication and Characterization of Two-Photon Polymerized Features in Colloidal Crystals. Adv Funct Mater. 2005;15:1995-2004.
Radic Z, Pickering NA, Vellom DC, Camp S, Taylor P. Three distinct domains in the cholinesterase molecule confer selectivity for acetyl-and butyrylcholinesterase inhibitors. Biochemistry. 1993;32:12074-84.
Reese CE, Asher SA. Photonic crystal optrode sensor for detection of Pb2+ in high ionic strength environments. Analytical chemistry. 2003;75:3915-8.
Reese CE, Guerrero CD, Weissman JM, Lee K, Asher SA. Synthesis of highly charged, monodisperse polystyrene colloidal particles for the fabrication of photonic crystals. J Colloid Interface Sci. 2000;232:76-80.
Richert L, Lavalle P, Vautier D, Senger B, Stoltz J-F, Schaaf P, et al. Cell interactions with polyelectrolyte multilayer films. Biomacromolecules. 2002;3:1170-8.
Roche. Annual Report, F. Hoffmann-La Roche AG. 2014.
Rochon PL, Lévesque L. Standing wave surface plasmon mediated forward and backward scattering. Opt Express. 2006;14:13050-5.
Rodríguez-Fernández J, Fedoruk M, Hrelescu C, Lutich AA, Feldmann J. Triggering the volume phase transition of core–shell Au nanorod–microgel nanocomposites with light. Nanotechnology. 2011;22:245708.
Rooney MTV, Seitz WR. An optically sensitive membrane for pH based on swellable polymer microspheres in a hydrogel. Anal Commun. 1999;36:267-70.
Rosen S. The Worldwide Market for In Vitro Diagnostic (IVD) Tests, 9th Ed., Kalomara Information. 2014.
Rundquist PA, Photinos P, Jagannathan S, Asher SA. Dynamical Bragg diffraction from crystalline colloidal arrays. The Journal of Chemical Physics. 1989;91:4932-41.
Sai N, Ning B, Huang G, Wu Y, Zhou Z, Peng Y, et al. An imprinted crystalline colloidal array chemical-sensing material for detection of trace diethylstilbestrol. Analyst. 2013;138:2720-8.
Saito H, Takeoka Y, Watanabe M. Simple and precision design of porous gel as a visible indicator for ionic species and concentration. Chem Commun (Cambridge, U K). 2003:2126-7.
Sartain FK, Yang XP, Lowe CR. Holographic lactate sensor. Anal Chem. 2006;78:5664-70.
Sartain FK, Yang XP, Lowe CR. Complexation of L-lactate with boronic acids: A solution and holographic analysis. Chem Eur J. 2008;14:4060-7.
Schild H. Poly (N-isopropylacrylamide): experiment, theory and application. Prog Polym Sci. 1992;17:163-249.
Schönhoff M. Self-assembled polyelectrolyte multilayers. Curr Opin Colloid Interface Sci. 2003;8:86-95.
Serpe MJ, Kim J, Lyon LA. Colloidal hydrogel microlenses. Adv Mater. 2004;16:184-7.
Shakhsher Z, Seitz WR, Legg KD. Single fiber-optic pH sensor based on changes in reflection accompanying polymer swelling. Anal Chem. 1994;66:1731-5.
Sharma AC, Jana T, Kesavamoorthy R, Shi L, Virji MA, Finegold DN, et al. A general photonic crystal sensing motif: creatinine in bodily fluids. Journal of the American Chemical Society. 2004;126:2971-7.
Shields D, Sale A. Global in Vitro Diagnostics (IVD) Market (Technique, Product, Usability, Application, End User, and Geography) - Size, Share, Global Trends, Company Profiles, Demand, Insights, Analysis, Research, Report, Opportunities, Segmentation and Forecast, 2013 - 2020, Allied Market Research. 2014.

Shimamoto C, Hirata I, Katsu K. Breath and blood ammonia in liver cirrhosis. Hepato-gastroenterology. 1999;47:443-5.
Shimazaki Y, Mitsuishi M, Ito S, Yamamoto M. Preparation of the layer-by-layer deposited ultrathin film based on the charge-transfer interaction. Langmuir. 1997;13:1385-7.
Siemens. Annual Report, Siemens. 2014.
Singh S, Gupta BD. Fabrication and characterization of a highly sensitive surface plasmon resonance based fiber optic pH sensor utilizing high index layer and smart hydrogel. Sens Actuators, B. 2012;173:268-73.
Specht EH, Neuman A, Hills N, Neher HT. Preparation of acrylamides. 1956.
Spooncer RC, Al-Ramadhan FAS, Jones BE. A Humidity Sensor Using a Wavelength-Dependent Holographic Filter with Fibre Optic Links. Int J Optoelectron. 1992;7:449-52.
Springsteen G, Wang B. A detailed examination of boronic acid–diol complexation. Tetrahedron. 2002;58:5291-300.
St John A, Price CP. Existing and emerging technologies for point-of-care testing. Clin Biochem Rev. 2014;35:155.
Stuart MAC, Huck WT, Genzer J, Müller M, Ober C, Stamm M, et al. Emerging applications of stimuli-responsive polymer materials. Nat Mater. 2010;9:101-13.
Sun J, Wu T, Sun Y, Wang Z, Zhang X, Shen J, et al. Fabrication of a covalently attached multilayer via photolysis of layer-by-layer self-assembled films containing diazo-resins. Chem Commun (Cambridge, U K). 1998:1853-4.
Taguchi Y, Takano E, Takeuchi T. SPR Sensing of Bisphenol A Using Molecularly Imprinted Nanoparticles Immobilized on Slab Optical Waveguide with Consecutive Parallel Au and Ag Deposition Bands Coexistent with Bisphenol A-Immobilized Au Nanoparticles. Langmuir. 2012;28:7083-8.
Takeoka Y, Watanabe M. Template Synthesis and Optical Properties of Chameleonic Poly (N-isopropylacrylamide) Gels Using Closest-Packed Self-Assembled Colloidal Silica Crystals. Adv Mater. 2003;15:199-201.
Takeoka Y, Watanabe M, Yoshida R. Self-sustaining peristaltic motion on the surface of a porous gel. J Am Chem Soc. 2003;125:13320-1.
Tan EV, Lowe CR. Holographic Enzyme Inhibition Assays for Drug Discovery. Anal Chem. 2009;81:7579-89.
Tétreault N, Mihi A, Míguez Hn, Rodríguez I, Ozin GA, Meseguer F, et al. Dielectric planar defects in colloidal photonic crystal films. Adv Mater. 2004;16:346-9.
Tétreault N, von Freymann G, Deubel M, Hermatschweiler M, Pérez-Willard F, John S, et al. New Route to Three-Dimensional Photonic Bandgap Materials: Silicon Double Inversion of Polymer Templates. Adv Mater. 2006;18:457-60.
Tian T, Li X, Cui J, Li J, Lan Y, Wang C, et al. Highly Sensitive Assay for Acetylcholinesterase Activity and Inhibition Based on a Specifically Reactive Photonic Nanostructure. ACS Appl Mater Interfaces. 2014;6:15456-65.
Tikhonov A, Kornienko N, Zhang J-T, Wang L, Asher SA. Reflectivity enhanced two-dimensional dielectric particle array monolayer diffraction. J Nanophotonics. 2012;6:063509-1--9.
Tokareva I, Minko S, Fendler JH, Hutter E. Nanosensors Based on Responsive Polymer Brushes and Gold Nanoparticle Enhanced Transmission Surface Plasmon Resonance Spectroscopy. J Am Chem Soc. 2004;126:15950-1.

Tokareva I, Tokarev I, Minko S, Hutter E, Fendler JH. Ultrathin molecularly imprinted polymer sensors employing enhanced transmission surface plasmon resonance spectroscopy. Chem Commun (Cambridge, U K). 2006:3343-5.
Tonyushkina K, Nichols JH. Glucose meters: a review of technical challenges to obtaining accurate results. J Diabetes Sci Technol. 2009;3:971-80.
Trope I, Lopez-Villegas D, Cecil KM, Lenkinski RE. Exposure to lead appears to selectively alter metabolism of cortical gray matter. Pediatrics. 2001;107:1437-43.
Tsangarides CP, Yetisen AK, Vasconcellos FD, Montelongo Y, Qasim MM, Wilkinson TD, et al. Computational modelling and characterisation of nanoparticle-based tuneable photonic crystal sensors. RSC Adv. 2014;4:10454-61.
Ueno K, Matsubara K, Watanabe M, Takeoka Y. An Electro- and Thermochromic Hydrogel as a Full-Color Indicator. Adv Mater. 2007;19:2807-12.
Um SH, Lee JB, Park N, Kwon SY, Umbach CC, Luo D. Enzyme-catalysed assembly of DNA hydrogel. Nat Mater. 2006;5:797-801.
Urbas A, Fink Y, Thomas EL. One-dimensionally periodic dielectric reflectors from self-assembled block copolymer-homopolymer blends. Macromolecules. 1999;32:4748-50.
Urbas AM, Maldovan M, DeRege P, Thomas EL. Bicontinuous cubic block copolymer photonic crystals. Adv Mater. 2002;14:1850-3.
Vasconcellos FdC, Yetisen AK, Montelongo Y, Butt H, Grigore A, Davidson CA, et al. Printable surface holograms via laser ablation. ACS Photonics. 2014;1:489-95.
Vekris E, Kitaev V, von Freymann G, Perovic DD, Aitchison JS, Ozin GA. Buried linear extrinsic defects in colloidal photonic crystals. Adv Mater. 2005;17:1269-72.
Verma R, Gupta BD. Fiber optic SPR sensor for the detection of 3-pyridinecarboxamide (vitamin B3) using molecularly imprinted hydrogel. Sens Actuators, B. 2013;177:279-85.
Vignolini S, Rudall PJ, Rowland AV, Reed A, Moyroud E, Faden RB, et al. Pointillist structural color in Pollia fruit. Proceedings of the National Academy of Sciences of the United States of America. 2012;109:15712-5.
Volpatti LR, Yetisen AK. Commercialization of microfluidic devices. Trends Biotechnol. 2014;32:347-50.
von Freymann G, Kitaev V, Lotsch BV, Ozin GA. Bottom-up assembly of photonic crystals. Chem Soc Rev. 2013;42:2528-54.
Vukusic P, Sambles JR. Photonic structures in biology. Nature. 2003;424:852-5.
Walker JP, Asher SA. Acetylcholinesterase-based organophosphate nerve agent sensing photonic crystal. Analytical chemistry. 2005;77:1596-600.
Wang P, Zhang L, Xia Y, Tong L, Xu X, Ying Y. Polymer nanofibers embedded with aligned gold nanorods: a new platform for plasmonic studies and optical sensing. Nano Lett. 2012;12:3145-50.
Wang Z, Zhang J, Li J, Xie J, Li Y, Liang S, et al. Colorful detection of organic solvents based on responsive organic/inorganic hybrid one-dimensional photonic crystals. J Mater Chem. 2011;21:1264-70.
Wei Chang W, Chi Chiu C, Yi Fan Z, Kam Chew L. Miniature Single-Mode Fiber Refractive Index Interferometer Sensor Based on High Order Cladding Mode and Core-Offset. IEEE Photonics Technol Lett. 2012;24:359-61.
Wichterle O, Lim D. Hydrophilic gels for biological use. 1960.
Wong WC, Chan CC, Hu P, Chan JR, Low YT, Dong X, et al. Miniature pH optical fiber sensor based on waist-enlarged bitaper and mode excitation. Sens Actuators, B. 2014;191:579-85.

Worsley GJ, Tourniaire GA, Medlock KE, Sartain FK, Harmer HE, Thatcher M, et al. Continuous blood glucose monitoring with a thin-film optical sensor. Clin Chem. 2007;53:1820-6.
Worsley GJ, Tourniaire GA, Medlock KE, Sartain FK, Harmer HE, Thatcher M, et al. Measurement of glucose in blood with a phenylboronic acid optical sensor. J Diabetes Sci Technol. 2008;2:213-20.
Wulff G. Molecular imprinting in cross-linked materials with the aid of molecular templates—a way towards artificial antibodies. Angew Chem, Int Ed Engl. 1995;34:1812-32.
Xia Y, Gates B, Yin Y, Lu Y. Monodispersed colloidal spheres: old materials with new applications. Adv Mater. 2000;12:693-713.
Xiao X-C, Chu L-Y, Chen W-M, Wang S, Xie R. Preparation of Submicrometer-Sized Monodispersed Thermoresponsive Core−Shell Hydrogel Microspheres. Langmuir. 2004;20:5247-53.
Xing J-F, Zheng M-L, Duan X-M. Two-photon polymerization microfabrication of hydrogels: an advanced 3D printing technology for tissue engineering and drug delivery. Chem Soc Rev. 2015;44:5031-9.
Xue F, Meng Z, Qi F, Xue M, Wang F, Chen W, et al. Two-dimensional inverse opal hydrogel for pH sensing. Analyst. 2014a;139:6192-6.
Xue F, Meng Z, Wang Y, Huang S, Wang Q, Lu W, et al. A molecularly imprinted colloidal array as a colorimetric sensor for label-free detection of p-nitrophenol. Anal Methods. 2014b;6:831-7.
Yang X, Lee MC, Sartain F, Pan X, Lowe CR. Designed boronate ligands for glucose-selective holographic sensors. Chemistry. 2006;12:8491-7.
Yang XP, Pan XH, Blyth J, Lowe CR. Towards the real-time monitoring of glucose in tear fluid: Holographic glucose sensors with reduced interference from lactate and pH. Biosens Bioelectron. 2008;23:899-905.
Ye B-F, Zhao Y-J, Li T-T, Xie Z-Y, Gu Z-Z. Aptamer-based suspension array indexed by structural color and shape. J Mater Chem. 2011;21:18659-64.
Yee CK, Jordan R, Ulman A, White H, King A, Rafailovich M, et al. Novel one-phase synthesis of thiol-functionalized gold, palladium, and iridium nanoparticles using superhydride. Langmuir. 1999;15:3486-91.
Yeo SJ, Tu F, Kim S-h, Yi G-R, Yoo PJ, Lee D. Angle-and strain-independent coloured free-standing films incorporating non-spherical colloidal photonic crystals. Soft matter. 2015;11:1582-8.
Yetisen AK. Fundamentals of Holographic Sensing. Cham, Switzerland: Springer International Publishing; 2015a. p. 27-51.
Yetisen AK. Holographic Glucose Sensors. Holographic Sensors. Cham, Switzerland: Springer International Publishing; 2015b. p. 101-34.
Yetisen AK. Holographic Metal Ion Sensors. Holographic Sensors. Cham, Switzerland: Springer International Publishing; 2015c. p. 85-99.
Yetisen AK. Holographic pH Sensors. Holographic Sensors. Cham, Switzerland: Springer International Publishing; 2015d. p. 53-83.
Yetisen AK. Mobile Medical Applications. Holographic Sensors. Cham, Switzerland: Springer International Publishing; 2015e. p. 135-48.
Yetisen AK. Point-of-Care Diagnostics. Holographic Sensors. Cham, Switzerland: Springer International Publishing; 2015f. p. 1-25.

Yetisen AK. The Prospects for Holographic Sensors. Holographic Sensors. Cham, Switzerland: Springer International Publishing; 2015g. p. 149-62.
Yetisen AK, Akram MS, Lowe CR. Paper-based microfluidic point-of-care diagnostic devices. Lab Chip. 2013;13:2210-51.
Yetisen AK, Butt H, Vasconcellos FD, Montelongo Y, Davidson CAB, Blyth J, et al. Light-Directed Writing of Chemically Tunable Narrow-Band Holographic Sensors. Adv Opt Mater. 2014a;2:250-4.
Yetisen AK, Martinez-Hurtado JL, da Cruz Vasconcellos F, Simsekler MCE, Akram MS, Lowe CR. The regulation of mobile medical applications. Lab Chip. 2014b;14:833-40.
Yetisen AK, Martinez-Hurtado JL, Garcia-Melendrez A, da Cruz Vasconcellos F, Lowe CR. A smartphone algorithm with inter-phone repeatability for the analysis of colorimetric tests. Sens Actuators, B. 2014c;196:156-60.
Yetisen AK, Montelongo Y, da Cruz Vasconcellos F, Martinez-Hurtado JL, Neupane S, Butt H, et al. Reusable, robust, and accurate laser-generated photonic nanosensor. Nano Lett. 2014d;14:3587-93.
Yetisen AK, Montelongo Y, Farandos NM, Naydenova I, Lowe CR, Yun SH. Mechanism of multiple grating formation in high-energy recording of holographic sensors. Appl Phys Lett. 2014e;105:261106.
Yetisen AK, Montelongo Y, Qasim MM, Butt H, Wilkinson TD, Monteiro MJ, et al. Photonic Nanosensor for Colorimetric Detection of Metal Ions. Anal Chem. 2015a;87:5101-8.
Yetisen AK, Naydenova I, da Cruz Vasconcellos F, Blyth J, Lowe CR. Holographic sensors: three-dimensional analyte-sensitive nanostructures and their applications. Chem Rev. 2014f;114:10654-96.
Yetisen AK, Qasim MM, Nosheen S, Wilkinson TD, Lowe CR. Pulsed laser writing of holographic nanosensors. J Mater Chem C. 2014g;2:3569.
Yetisen AK, Volpatti LR. Patent protection and licensing in microfluidics. Lab Chip. 2014;14:2217-25.
Yetisen AK, Volpatti LR, Coskun AF, Cho S, Kamrani E, Butt H, et al. Entrepreneurship. Lab Chip. 2015b;15:3638-60.
Yoo PJ, Nam KT, Qi J, Lee S-K, Park J, Belcher AM, et al. Spontaneous assembly of viruses on multilayered polymer surfaces. Nat Mater. 2006;5:234-40.
Yoon J, Lee W, Thomas EL. Thermochromic block copolymer photonic gel. Macromolecules. 2008;41:4582-4.
Young T. Experimental demonstration of the general law of the interference of light. Phil Trans R Soc Lond. 1804;94:1-16.
Yuan Y, Li Z, Liu Y, Gao J, Pan Z, Liu Y. Hydrogel Photonic Sensor for the Detection of 3-Pyridinecarboxamide. Chemistry – A European Journal. 2012;18:303-9.
Zaarour M, Dong B, Naydenova I, Retoux R, Mintova S. Progress in zeolite synthesis promotes advanced applications. Microporous Mesoporous Mater. 2014;189:11-21.
Zeng F, Wu S, Sun Z, Xi H, Li R, Hou Z. Urea sensing materials via solidified crystalline colloidal arrays. Sens Actuators, B. 2002;81:273-6.
Zeng X, Du Z, Ma J. Colorimetric detection of ultratrace cholesterol by free standing inverse opal hydrogel films. Optical Sensors. Monterey, CA: Optical Society of America; 2012. p. STh1B. 5.

Zhai L, Nolte AJ, Cohen RE, Rubner MF. pH-Gated Porosity Transitions of Polyelectrolyte Multilayers in Confined Geometries and Their Application as Tunable Bragg Reflectors. Macromolecules. 2004;37:6113-23.
Zhang C, Losego MD, Braun PV. Hydrogel-based glucose sensors: effects of phenylboronic acid chemical structure on response. Chem Mater. 2013a;25:3239-50.
Zhang J-T, Chao X, Liu X, Asher SA. Two-dimensional array Debye ring diffraction protein recognition sensing. Chem Commun (Cambridge, U K). 2013b;49:6337-9.
Zhang M-L, Jin F, Zheng M-L, Duan X-M. Inverse opal hydrogel sensor for the detection of pH and mercury ions. RSC Adv. 2014;4:20567-72.
Zhang QM, Ahiabu A, Gao Y, Serpe MJ. CO2-switchable poly (N-isopropylacrylamide) microgel-based etalons. J Mater Chem C. 2015;3:495-8.
Zhao Q, Yetisen AK, Anthony CJ, Fowler WR, Yun SH, Butt H. Printable ink holograms. Appl Phys Lett. 2015a;107:041115.
Zhao Q, Yetisen AK, Sabouri A, Yun SH, Butt H. Printable Nanophotonic Devices via Holographic Laser Ablation. ACS Nano. 2015b;9:9062-9.
Zhao Y, Shang L, Cheng Y, Gu Z. Spherical Colloidal Photonic Crystals. Acc Chem Res. 2014;47:3632-42.
Zhao Y, Wostyn K, de Schaetzen G, Clays K, Hellemans L, Persoons A, et al. The fabrication of photonic band gap materials with a two-dimensional defect. Appl Phys Lett. 2003;82:3764-6.
Zhao Y, Xie Z, Gu H, Zhu C, Gu Z. Bio-inspired variable structural color materials. Chem Soc Rev. 2012;41:3297-317.
Zhao Y, Zhao X, Gu Z. Photonic crystals in bioassays. Adv Funct Mater. 2010a;20:2970-88.
Zhao Y, Zhao X, Tang B, Xu W, Gu Z. Rapid and Sensitive Biomolecular Screening with Encoded Macroporous Hydrogel Photonic Beads. Langmuir. 2010b;26:6111-4.
Zhao Y, Zhao X, Tang B, Xu W, Li J, Hu J, et al. Quantum-Dot-Tagged Bioresponsive Hydrogel Suspension Array for Multiplex Label-Free DNA Detection. Adv Funct Mater. 2010c;20:976-82.
Zhong Q, Xu H, Ding H, Bai L, Mu Z, Xie Z, et al. Preparation of conducting polymer inverse opals and its application as ammonia sensor. Colloids Surf, A. 2013;433:59-63.

View publication stats